

Search for Heavy Neutral Leptons with IceCube DeepCore

Dissertation
zur Erlangung des akademischen Grades
doctor rerum naturalium
(Dr. rer. nat.)

im Fach: Physik
Spezialisierung: Experimentalphysik

eingereicht an der
Mathematisch-Naturwissenschaftlichen Fakultät
der Humboldt-Universität zu Berlin

von
Leander Fischer M. Sc.
geboren am 24. Oktober 1992
in Heidelberg

Präsidentin der Humboldt-Universität zu Berlin
Prof. Dr. Julia von Blumenthal

Dekanin der Mathematisch-Naturwissenschaftlichen Fakultät
Prof. Dr. Caren Tischendorf

Copyright Notice

This book is released into the public domain using the CC-BY-4.0 code.

To view a copy of the CC-BY-4.0 code, visit:

<https://creativecommons.org/licenses/by/4.0/>

Colophon

This document was typeset with the help of KOMA-Script and L^AT_EX using the open-source kaobook template class.

The source code of this thesis is available at:

https://github.com/LeanderFischer/phd_thesis

Zusammenfassung

Zusammenfassung ...

Abstract

Abstract ...

Todo list

add fancy icecube picture	1
SB: there are more properties than just these. Somehow need a half sentence that explains why these are particularly important to single out (see ice papers for inspiration)	2
CL: maybe define that absorption and scattering lengths are? they are defined differently so this invites a comparison that is not so obvious	2
Add reference for the dust layer!	2
exchange for figure with scattering (check abs/sca is correct)	2
mention/cite dust logger paper/procedure?	2
Add accuracy of the efficiency calibration here.	3
Maybe throw the coordinate system in a box on the side?	3
Blow up this image a bit, so it's better readable as marginfigure.	3
CL: value?	4
SB: this needs revision. the energy range you mention is particular for oscillations already (atmopsheric neutrinos are plentiful outside of this range you mentioned). If you rewrite the first part you'll have to revisit the second part. Also in general I'd suggest not to rank analyses like Main and Other - DeepCore was orginally intended as a dark matter detector, and there are probably more DM analyses unblinded / year than oscillations. Just keep it general, no need to rank.	4
Cite n and θ_c	4
SB: you already mentioned that Cher. Rad. doesn't lead to signficant energy loss. I suggest to clean up the text a bit, you dont' need to emphasize that so many times. Pick one place (probably here) and eliminate it elsewhere	5
Add reference (PDG or find original)	5
SB: i like that you give a benchmark value here, for rule of thumb or so, but it should be related to the detector geometry somehow or else it feels too out of place. Give it some context	5
Add reference for these processes.	6
cite em shower distribution	6
Add angular profile plot (Summer agrees!) (create one based on Leif Rädel as Alex did)	6
SB: rephrase gamma (from equation) is not defined	6
SB: Explain	7
Make sure I have this defined in the SM interaction chapter!	8
SB: Since your analysis depends on the ability to reconstruct cascade directions, it seems odd to emphasize that the light is nearly isotropically emitted. Of course that is true, but the emphasis should rather be on the fact that there remains some assymetry to the light profile	8
Make my own DC string positions/distances plot version, viable for the margin?	9
Maybe just reference the one from the detector description and drop it here?	9
Re-make plot with all energies (cascades and total, both samples (they are the same))	10

Re-make plot with all decay lengths (both samples)	10
In which variables are they splined?	13
Re-make plot with 3 target masses and better labels/legends etc.	14
SB: emphasize the cut-off/suppression	14
Add comparisons of SM cross-sections between NuXSSplMkr and genie?	14
add varied total cross-section for a few background HNL events (for QE/RES variations?!?)	14
Calculate max BRs	15
JVS: consider also writing down the (trivial) 2-body decay kinematics for completeness and consistency. This transition is a bit jarring as it is	16
add table with number of gen level files? mention the event number is smaller because of kinematic condition?	17
Combine low/high plots and remove all traces of the separation in the thesis (tables/text/etc.)	18
maybe increase main text width? (read in kao docu)	19
Adapt to reflect switched chapter order	19
put a number on this significant increase?	23
put a number on the tilt angle?	24
Add SPE distribution plot	25
AT: Das klingt so, als würde die MC Simulation ein analoges Signal erzeugen, was auch digitalisiert wird. Vllt kann man das nochmal nachforschen, aber zumindest in meiner Arbeit habe ich geschrieben, dass die MCPEs direkt in ATWD und fADC Readouts umgewandelt werden.	25
add example plots (2?) for L3 cut variables and applied cuts	27
add some figure showing the corridors?	28
add table with rates per level (split in flavor) - maybe better in analysis chapter to also show signal? . .	28
add image with selected strings used for flercnn IC and DC	29
add some performance plots of the FLERCNN reconstruction	29
There is more information on pre-processing the samples and preparing the input features, and training each cnn, but I'm not sure if that might be too much detail?	29
add reference for flercnn analysis internal note	30
add final sample composition, but maybe also in analysis chapter to show signal and background? . .	31
at some place I will want a selection efficiency plot for SM BG and HNL signal, but I'm not sure where to put it yet	31
add figure with Barr blocks?	32
which experiments measure the axial mass?	33
cite this?	35
Re-make plot with x,y for horizontal set one plot!	39
Re-make plot with x, y, z for both cascades in one.	39
Re-arrange plots in a more sensible way.	39

Contents

Abstract	iii
Contents	vii
1 The IceCube Neutrino Observatory	1
1.1 Detector Components	1
1.1.1 Digital Optical Modules and the Antarctic Ice	2
1.1.2 IceCube	3
1.1.3 DeepCore	3
1.2 Particle Propagation in Ice	4
1.2.1 Cherenkov Effect	4
1.2.2 Energy Losses	5
1.3 Event Morphologies	7
2 Heavy Neutral Lepton Signal Simulation	9
2.1 Model Independent Simulation	9
2.1.1 Simplistic Samples	9
2.1.2 Realistic Sample	10
2.2 Model Dependent Simulation	12
2.2.1 Custom LeptonInjector	12
2.2.2 Sampling Distributions	16
2.2.3 Weighting Scheme	16
2.2.4 Generation Level Distributions	18
3 Standard Model Background Simulation and Data Processing	21
3.1 Event Generation	21
3.1.1 Neutrinos	22
3.1.2 Muons	23
3.2 Detector Simulation	23
3.2.1 Photon Propagation	24
3.2.2 Detector Responses	24
3.3 Processing	25
3.3.1 Trigger and Filter	25
3.3.2 Event Selection	27
3.4 Reconstruction	29
3.4.1 Fast Low Energy Reconstruction using Convolutional Neural Networks	29
3.4.2 Analysis Selection	30
3.5 Systematic Uncertainties	31
3.5.1 Atmospheric Flux Uncertainties	32
3.5.2 Cross-Section Uncertainties	32
3.5.3 Detector Calibration Uncertainties	33
3.5.4 Muon Uncertainties	34
APPENDIX	37
A Heavy Neutral Lepton Signal Simulation	39
A.1 Model Independent Simulation Distributions	39
A.2 Model Dependent Simulation Distributions	40

B Analysis Checks	41
B.1 Minimization Robustness	41
B.1.1 Ensemble Tests	41
Bibliography	43

List of Figures

1.1	IceCube overview	1
1.2	IceCube sideview	2
1.3	Digital Optical Module (DOM)	3
1.4	IceCube top view	3
1.5	Cherenkov light front	4
2.1	DeepCore string spacing	10
2.2	Simplified model independent simulation generation level distributions	11
2.3	Realistic model independent simulation generation level distributions	12
2.4	HNL branching ratios	13
2.5	Custom HNL total cross-sections for the four target masses compared to the total ($\nu_\tau/\bar{\nu}_\tau$ NC) cross-section used for SM neutrino simulation production with GENIE.	14
2.6	Model dependent simulation generation level distributions	18
3.1	Depth dependent scattering and absorption lengths	24
3.2	IceCube trigger efficiencies	26
3.3	Level 4 classifier outputs (muon and noise)	28
3.4	FLERCNN architecture	30
3.5	FLERCNN muon classifier probability distributions	31
3.6	Inclusive total neutrino-nucleon cross-sections	34
3.7	Hole ice angular acceptance modification	35
A.1	Simplified model independent simulation generation level distributions	39
A.2	Realistic model independent simulation generation level distributions	40
A.3	Model dependent simulation generation level distributions	40
B.1	Asimov inject/recover test (0.3 GeV, 1.0 GeV)	41
B.2	Pseudo-data trials TS distribution (0.3 GeV, 1.0 GeV)	41

List of Tables

1.1	IceCube low energy event signatures and underlying interactions	7
2.1	Simplified model independent simulation sampling distributions	11
2.2	Realistic model independent simulation sampling distributions	12
2.3	HNL mass dependent decay channels	15
2.4	Model dependent simulation sampling distributions	16
3.1	GENIE generation cylinder volumes	22
3.2	Vuvuzela noise simulation parameters	25
3.3	Final analysis cuts	31

The IceCube Neutrino Observatory

1

The IceCube Neutrino Observatory [1] is a cubic-kilometer, ice-Cherenkov detector located at the geographic South Pole. IceCube utilizes the Antarctic glacial ice as detector medium to observe neutrinos by measuring the Cherenkov light produced from secondary charged particles. It was deployed between 2006 and 2011 and has been taking data since the installation of the first modules. The primary goal of IceCube is the observation of astrophysical neutrinos as a telescope, but it can also be used to study fundamental particle physics properties by measuring atmospheric neutrinos as well as studying cosmic rays.

This chapter first describes the main- and sub-array of the detector and its detection module in Section 1.1, the propagation of particles through ice is explained in Section 1.2, and finally, the signatures that IceCube can observe of the different particles are introduced in Section 1.3.

add fancy icecube picture	
1.1 Detector Components	1
1.2 Particle Propagation in Ice	4
1.3 Event Morphologies	7

[1]: Aartsen et al. (2017), "The IceCube Neutrino Observatory: instrumentation and online systems"

1.1 Detector Components

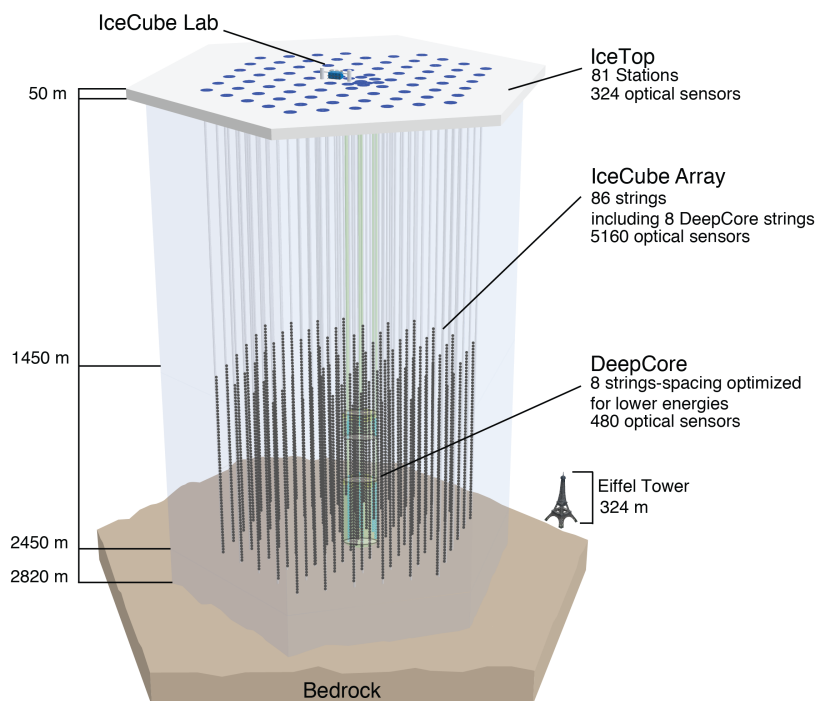


Figure 1.1: Overview of the IceCube detector showing the in-ice main- and sub-array IceCube and DeepCore, IceTop, and the IceCube Laboratory. From [1].

The full IceCube detector array consists of 86 vertical, in-ice strings and 81 surface stations as shown in Figure 1.1. The in-ice part is composed of 60 optical modules per string deployed at depths of 1450 m–2450 m below the ice, while the surface stations of the cosmic air-shower array, *IceTop*, are ice-filled tanks. The surface stations and the majority of the strings are arranged in a hexagonal grid with the operations building, the *IceCube Laboratory* (ICL), central to the grid on the surface. A top view

of the hexagonal arrangement is shown in Figure 1.4. The in-ice array is designed to detect neutrinos in the energy range from GeV to PeV.

1.1.1 Digital Optical Modules and the Antarctic Ice

[2]: Price et al. (2000), "Age vs depth of glacial ice at South Pole"

SB: there are more properties than just these. Somehow need a half sentence that explains why these are particularly important to single out (see ice papers for inspiration)

CL: maybe define that absorption and scattering lengths are? they are defined differently so this invites a comparison that is not so obvious

[3]: Abbasi et al. (2022), "In-situ estimation of ice crystal properties at the South Pole using LED calibration data from the IceCube Neutrino Observatory"

Add reference for the dust layer!

Figure 1.2: Side view of IceCube and DeepCore showing the depth dependent scattering and absorption length (left panel) and the DOM positions around the dust layer.

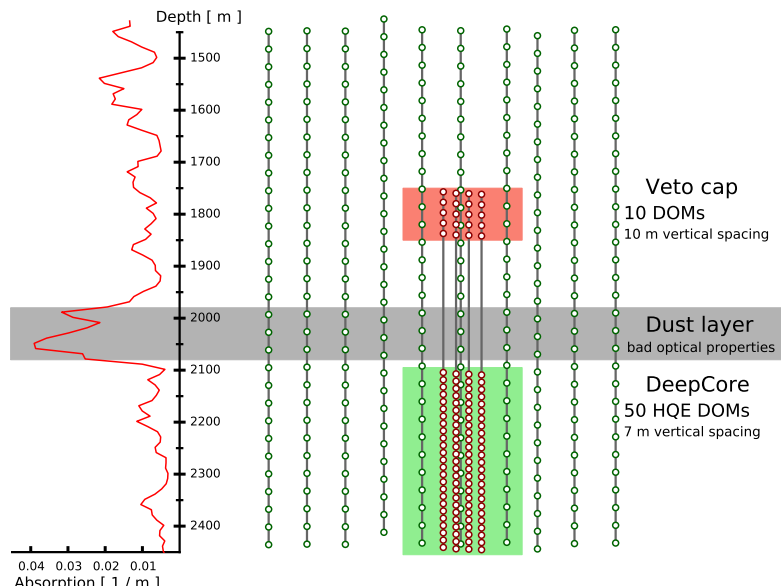
exchange for figure with scattering (check abs/sca is correct)

mention/cite dust logger paper/procedure?

[4]: Abbasi et al. (2009), "The IceCube data acquisition system: Signal capture, digitization, and timestamping"

[4]: Abbasi et al. (2009), "The IceCube data acquisition system: Signal capture, digitization, and timestamping"

The IceCube detection medium is the Antarctic glacial ice itself, which was formed over 100 000 years by accumulation of snow that was subsequently compressed by its own weight to form a dense crystal structure [2]. As a result of this formation process, the optical properties, scattering and absorption, primarily change with depth. Within the detector volume the absorption length ranges from 100 m-400 m, while the scattering length lies between 20 m and 100 m. They are correlated, with the absorption length being roughly four times the scattering length [3]. The vertical distribution of scattering and absorption length can be seen in Figure 1.2, where one dominant feature is the *dust layer* between 2000 m and 2100 m depth. This region has a higher concentration of dust particles that were deposited in a period of high volcanic activity, which leads to bad optical properties in form of larger scattering and absorption.



The ice is instrumented by 5160 optical sensors called *Digital Optical Modules* (DOMs) [4], which can detect the Cherenkov light produced by charged particles traveling through the ice. Each DOM is made of a spherical glass housing, containing a downward-facing Photomultiplier Tube (PMT), the main-board with control, readout, and processing-electronics, and a LED flasher-board for calibration purposes. The design and the individual components of a DOM can be seen in Figure 1.3.

The majority of PMTs are the 10" Hamamatsu R7081-02, which have a bialkali photocathode and are sensitive to wavelengths in the range of 300 nm to 650 nm, with a peak quantum efficiency of 25% at 390 nm. In the central part of the IceCube array the peak efficiency reaches 34%. The dark count rate in the temperature range of -40°C to -20°C is ~ 300 Hz. The DOM electronics measure the PMT voltage and control the gain. At a voltage crossing of the equivalent to 0.25 PE the waveform readout is activated [4]. Only when either one of the nearest or next to nearest

DOMs above or below also sees a voltage crossing within a 1 μ s time window¹, the voltages are digitized and sent to the ICL. Through the application of a waveform unfolding algorithm, called *WaveDeform* [5], the waveforms are compressed, and the results are the reconstructed times and charges of the photo-electrons. This is the basis for all further IceCube data processing.

The PMT is covered with a mu-metal grid (made from wire mesh), shielding the photocathode from Earth's magnetic field, and it is optically coupled to the glass sphere by RTV silicone gel. The glass sphere is a pressure vessel, designed to withstand both the constant ice pressure and the temporary pressure during the refreezing process of the water in the drill hole during deployment (peaking at around 690 bar). The sphere is held by a harness that connects the DOMs along a string and also guides the cable beside them.

The flasher-board controls 12 LEDs that produce optical pulses with a wavelength of 405 nm [1]. The LEDs can be pulsed separately or in combination with variable output levels and pulse lengths. Using the known information of the light source positions and times this can be used for in-situ calibration of the detector by measuring absorption and scattering properties of the ice. Calibrating the absolute efficiency of the DOMs itself is more accurately done using minimum ionizing muons [6, 7], since the total amplitude of the LED light is not well known.

1.1.2 IceCube

The 78 strings that are arranged in a hexagonal pattern from the main part of the in-ice array, which is called *IceCube*. With a ~125 m horizontal spacing between the strings and a ~17 m vertical spacing between DOMs, IceCube has a lower energy threshold of around 100 GeV. IceCube was designed to detect astrophysical neutrinos with energies above 1 TeV.

The coordinate system that is used in IceCube is centered at 46500'E, 52200'N at an elevation of 883.9 m [1]. Per definition, it's a right-handed coordinate system where the y-axis points along the Prime Meridian (Grid North) towards Greenwich, UK, and the x-axis points 90° clockwise from the y-axis (Grid East). The z-axis is normal to the ice surface, pointing upwards. For IceCube analyses depth is defined as the distance along the z axis from the ice surface, assumed to be at an elevation of 2832 m.

1.1.3 DeepCore

The additional 8 strings form a denser sub-array of IceCube called *DeepCore* [8]. It's located at the bottom-center of the in-ice array and its *fiducial volume* also includes the 7 surrounding IceCube strings as shown in Figure 1.4. The strings in this region have a closer average horizontal distance of about 70 m. The lower 50 DeepCore DOMs on each string are placed in the region of clear ice below the dust layer between 2100 m to 2450 m depth, where their vertical spacing is ~7 m. The remaining 10 modules on each string are placed above the dust layer to be used as veto against atmospheric muons as can be seen in Figure 1.2. Additionally, the

1: This is referred to as a *hard local coincidence (HLC)* [4].

[5]: Aartsen et al. (2014), "Energy Reconstruction Methods in the IceCube Neutrino Telescope"

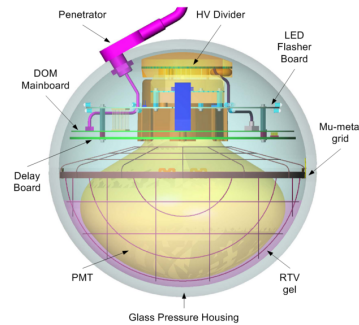


Figure 1.3: Design and components of a Digital Optical Module (DOM) [4]

[1]: Aartsen et al. (2017), "The IceCube Neutrino Observatory: instrumentation and online systems"

[6]: Feintzeig (2014), "Searches for Point-like Sources of Astrophysical Neutrinos with the IceCube Neutrino Observatory"

[7]: Kulacz (2019), "In Situ Measurement of the IceCube DOM Efficiency Factor Using Atmospheric Minimum Ionizing Muons"

Add accuracy of the efficiency calibration here.

[1]: Aartsen et al. (2017), "The IceCube Neutrino Observatory: instrumentation and online systems"

Maybe throw the coordinate system in a box on the side?

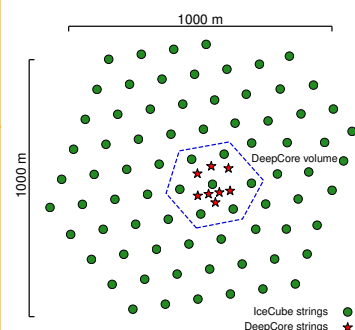


Figure 1.4: Top view of the IceCube array.

Blow up this image a bit, so it's better readable as marginfigure.

[8]: Abbasi et al. (2012), "The design and performance of IceCube DeepCore"

CL: value?

SB: this needs revision. the energy range you mention is particular for oscillations already (atmopsheric neutrinos are plentiful outside of this range you mentioned). If you rewrite the first part you'll have to revisit the second part. Also in general I'd suggest not to rank analyses like Main and Other - DeepCore was orginally intended as a dark matter detector, and there are probably more DM analyses unblinded / year than oscillations. Just keep it general, no need to rank.

[9]: Cherenkov (1937), "Visible Radiation Produced by Electrons Moving in a Medium with Velocities Exceeding that of Light"

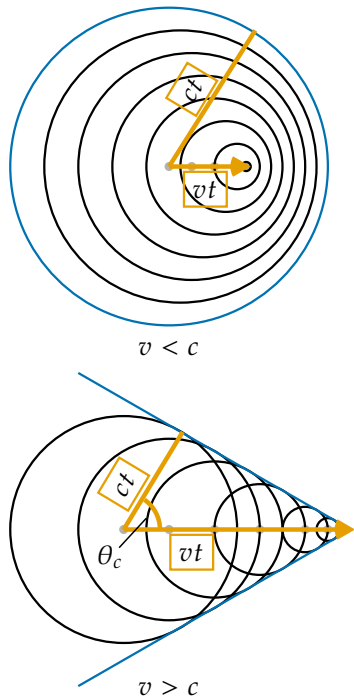


Figure 1.5: Schematic depiction of the spherical light front produced by a particle traveling slower than the speed of light in the medium (top) and the formation of the Cherenkov light front produced by a charged particle traveling faster than the speed of light in the medium (bottom). Blue is the resulting wavefront, while the black circles are spherically emitted light at each position and the orange arrows show the direction of the particle.

DeepCore DOMs are equipped with higher quantum efficiency PMTs. The combination of the denser spacing, the high quantum efficiency modules, and the most favorable ice properties below the dust layer leads to a lower energy detection threshold of around 5 GeV, allowing the more efficient observation of atmospheric neutrinos, which are mostly in the energy range of 10 GeV-100 GeV. The main analysis performed with DeepCore is an atmospheric neutrino oscillation measurement, but the large flux of atmospheric neutrinos allows for many other Beyond Standard Model searches, such as searches for dark matter, non-standard interactions, or sterile neutrinos.

1.2 Particle Propagation in Ice

Neutrinos interacting in the ice via DIS produce muons, electromagnetic showers, and hadronic showers, depending on their flavor and the interaction type. The particles produced in those processes mainly lose their energy through *ionization*, *bremsstrahlung*, *pair production*, and the *photo-nuclear interaction*. Electrically charged particles also emit Cherenkov light when traveling through the ice, which is the main observable in IceCube, but only contributes a small amount to the total energy loss. The Cherenkov effect and the energy losses of the particles are described in the following sections, followed by an overview of the different particle signatures in IceCube.

1.2.1 Cherenkov Effect

When a charged particle moves through a medium with a velocity that is greater than the speed of light in that medium, it emits Cherenkov radiation, losing a very small amount of energy ($\mathcal{O}(10^{-4})$ of the total energy loss). The detection principle of IceCube DeepCore, is based on the observation of resulting Cherenkov photons that are emitted by the charged secondary particles produced in the neutrino interactions that were introduced in Section ???. The Cherenkov effect was first observed by Pavel Cherenkov in 1934 [9] and occurs when the charged particle travels faster than the phase velocity of light, therefore polarizing the medium. Upon de-excitation the molecules emit the received energy as photons in a spherical wavefront. Since the particle moves past this wavefront, the superposition of the spherical light emissions forms a cone, which is shown in blue in the bottom panel of Figure 1.5.

Using trigonometry, the angle θ_c at which the Cherenkov light is emitted can be calculated as

$$\theta_c = \arccos\left(\frac{1}{\beta n}\right), \quad (1.1)$$

where β is the velocity of the particle in units of the speed of light and n is the refractive index of the medium. When the particle velocity is close to the speed of light, the equation holds and the angle is only dependent on the refractive index of the medium. For the Antarctic ice, the refractive index is $n \approx 1.3$ and as a result $\theta_c \approx 41^\circ$.

The frequency of the emission depends on the charge z and the wavelength-dependent index of refraction $n(\omega)$ and is given by the Frank-Tamm

formula [10, 11]

$$\frac{d^2N}{dx d\lambda} = \frac{2\pi\alpha z^2}{\lambda^2} \left(1 - \frac{1}{\beta^2 n(\omega)^2}\right), \quad (1.2)$$

with $\alpha \approx 1/137$ the fine structure constant, λ the wavelength of the emitted light, and x the path length traversed by the particle. Relativistic particles in ice produce roughly 250 photons per cm in the wavelength range of 300 nm-500 nm [12].

1.2.2 Energy Losses

Even though relativistic, charged particles traveling through matter produce Cherenkov radiation, their energy is mainly lost through other processes that are dependent on the particle type and energy. The exact principles of energy loss for the different types can broadly be categorized into the three groups: quasi-continuous energy loss by muons, electromagnetic cascades, and hadronic cascades.

Muons

Muons lose their energy by ionization, bremsstrahlung, pair production, and the photo-nuclear effect. The energy loss by ionization is the dominant process for muons above 1 GeV and has a weak energy dependence given by

$$\left\langle -\frac{dE}{dx} \right\rangle = a_I(E) + b_R(E) \cdot E, \quad (1.3)$$

where E is the energy and $a_I(E)$ and $b_R(E) \cdot E$ are the energy loss by ionization and the combined radiative losses, respectively. In the energy range relevant for this work (10 GeV-100 GeV), the parameters a_I and b_R only depend on energy very weakly and can be approximated by constants. The energy loss is then given by

$$\left\langle -\frac{dE}{dx} \right\rangle = a + b \cdot E. \quad (1.4)$$

Based on this description, there is a critical energy which divides the regimes where ionization and radiative losses dominate. The critical energy is given by $E_{\text{crit}} = a/b$ and for muons in ice it is ~ 713 GeV (using $a \approx 2.59 \text{ MeV cm}^{-1}$ and $b \approx 3.63 \times 10^{-6} \text{ cm}^{-1}$ [13]). Since the energy range of interest is well below this critical energy, the range of a muon can easily be related to its energy by

$$\langle L \rangle = \frac{E_0}{a}. \quad (1.5)$$

Measuring the length of a muon track therefore allows for an estimation of its energy if the full track is contained within the instrumented volume of IceCube. Using the given numbers a 30 GeV muon travels ~ 116 m. This approximate treatment does not take into account the stochastic nature of some energy losses. Bremsstrahlung and photo-nuclear interactions for example rarely occur, but when they do, they deposit a large chunk of energy. A thorough investigation of the energy losses of muons in ice can be found in [14].

Cite n and θ_c

[10]: Frank et al. (1937), "Coherent visible radiation from fast electrons passing through matter"

[11]: Tamm (1991), "Radiation Emitted by Uniformly Moving Electrons"

[12]: Rädel et al. (2012), "Calculation of the Cherenkov light yield from low energetic secondary particles accompanying high-energy muons in ice and water with Geant4 simulations"

SB: you already mentioned that Cher. Rad. doesn't lead to significant energy loss. I suggest to clean up the text a bit, you don't need to emphasize that so many times. Pick one place (probably here) and eliminate it elsewhere

Add reference (PDG or find original)

[13]: Chirkov et al. (2004), "Propagating leptons through matter with Muon Monte Carlo (MMC)"

SB: i like that you give a benchmark value here, for rule of thumb or so, but it should be related to the detector geometry somehow or else it feels too out of place. Give it some context

[14]: Raedel (2012), "Simulation Studies of the Cherenkov Light Yield from Relativistic Particles in High-Energy Neutrino Telescopes with Geant4"

Electromagnetic Showers

Add reference for these processes.

Photons as well as electrons and positrons are produced either directly in neutrino interactions or in secondary particle interactions. Above a critical energy E_c , they lose their energy through repeated pair production and bremsstrahlung emission forming an expanding, electromagnetic shower profile. The particles' energy reduces with every interaction and their number increases until they fall below the critical energy where ionization and excitation of surrounding atoms become the dominant energy loss processes for electrons and positrons. For photons the remaining energy is lost through the Compton effect and the photoelectric effect. Below the critical energy no new shower particles are produced. Electromagnetic cascades can be characterized by the radiation length, X_0 , after which electrons/positrons reduced their energy to $1/e$ of their initial energy. For photons, it's equivalent to $7/9$ of the mean free path of pair production. The critical energy for ice is $E_c \approx 78$ MeV, with a radiation length of $X_0 \approx 39.3$ cm [15].

[15]: Tanabashi et al. (2018), "Review of Particle Physics"

cite em shower distribution

The radiation length governs the longitudinal shower profile and using $t = x/X_0$, the shower intensity can be described by

$$\frac{dE}{dt} = E_0 b \frac{(bt)^{a-1} e^{-bt}}{\Gamma(a)}, \quad (1.6)$$

[14]: Raedel (2012), "Simulation Studies of the Cherenkov Light Yield from Relativistic Particles in High-Energy Neutrino Telescopes with Geant4"

[16]: Agostinelli et al. (2003), "Geant4—a simulation toolkit"

Add angular profile plot (Summer agrees!) (create one based on Leif Rädel as Alex did)

SB: rephrase gamma (from equation) is not defined

where a and b are parameters that have to be estimated from experiment. Based on the work from [14], performed with Geant4 [16], the parameters for electromagnetic showers in ice are

$$e^- : a \approx 2.01 + 1.45 \log_{10}(E_0/\text{GeV}), b \approx 0.63, \quad (1.7a)$$

$$e^+ : a \approx 2.00 + 1.46 \log_{10}(E_0/\text{GeV}), b \approx 0.63, \quad (1.7b)$$

$$\gamma : a \approx 2.84 + 1.34 \log_{10}(E_0/\text{GeV}), b \approx 0.65. \quad (1.7c)$$

The maximum of the shower is at $t_{max} = (a - 1)/b$ and the Cherenkov emission of the charged particles produced in the shower is peaked around the Cherenkov angle, since they are produced in the forward direction.

Hadronic Showers

The breaking nucleus or any hadronic decay products from the neutrino DIS interactions always create a hadronic cascade. It is a result of secondary particles produced in strong interactions between the hadrons and the traversed matter. The charged particles produced in the shower will emit Cherenkov radiation, while neutral particles will be invisible to the detector. There is also an electromagnetic component of the shower, due to for example the decay of neutral pions into photons. Hadronic showers of the same energy as electromagnetic showers have larger fluctuations in energy deposition and shape, since they depend on the produced particle types. Hadrons also have a higher energy threshold for Cherenkov light production, because of their higher mass. Based on [14, 17], the visible electromagnetic fraction of hadronic showers can be

[14]: Raedel (2012), "Simulation Studies of the Cherenkov Light Yield from Relativistic Particles in High-Energy Neutrino Telescopes with Geant4"

[17]: Gabriel et al. (1994), "Energy dependence of hadronic activity"

parameterized as

$$F(E_0) = \frac{T_{\text{hadron}}}{T_{\text{EM}}} = 1 - (1 - f_0) \left(\frac{E_0}{E_s} \right)^{-m}, \quad (1.8)$$

where $T_{\text{hadron/EM}}$ is the total track length of a hadronic/electromagnetic shower with the same energy, f_0 is the ratio of hadronic and electromagnetic light yield, E_0 is the initial energy, and E_s is an energy scale. The parameter m is an arbitrary parameter. The ratio $F(E_0)$ increases with energy, but is always smaller than 1. The variance of this distribution is given by

$$\sigma_F(E_0) = \sigma_0 \log(E_0)^{-\gamma}. \quad (1.9)$$

The parameters m , E_s , and f_0 are fit from simulation. Cherenkov light from hadronic showers also peaks around the Cherenkov angle, but the angular distribution is more smeared out, due to the variations in particle type and their energy depositions.

SB: Explain

1.3 Event Morphologies

The event morphologies produced by particles detected in IceCube are combinations of the three energy loss types described in Section 1.2.2, e.g. *cascades* from electromagnetic and hadronic showers and elongated *tracks* from muons traveling through the detector. Table 1.1 gives an overview of the possible event signatures.

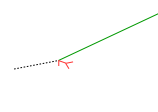
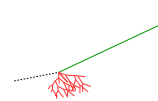
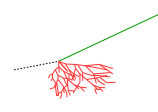
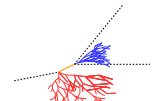
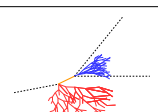
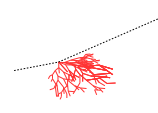
Interaction	Secondary particles	Signature
CC $\nu_\mu^{(-)}$	 μ^\pm track	Track-only
	 μ^\pm track and hadrons	Cascade + track
CC $\nu_\tau^{(-)}$	 τ^\pm decaying into μ^\pm (~17% BR), hadrons	
	 τ^\pm decaying into e^\pm or hadrons (~83% BR)	
CC $\nu_e^{(-)}$	 e^\pm , hadrons	Cascade-only
NC $\nu_\ell^{(-)}$	 hadrons	

Table 1.1: IceCube low energy event signatures, their underlying interaction type, and the particles that produce them. Also shown are the secondary particles produced in the interactions. Black dashed lines represent neutrinos, green lines muons, orange line leptons, and blue and red lines are particles in electromagnetic and hadronic cascades, respectively. Adapted from [18].

Neutrino interactions are observed as cascades, tracks, or a combination of both, depending on the initial flavor and the interaction type for the specific event.

In ν_μ - CC interactions, a muon is produced in addition to a hadronic shower from the breaking nucleus. If the interaction happens outside the detector, but the muon passes through the detector, this will create a track-like signature. The same happens if the interaction happens inside, but the energy transfer to the nucleus is small ($y \approx 0$). At energies relevant for this work, tracks have length at the same order of the distance between DOMs, so they can be observed as such.

Make sure I have this defined in the SM interaction chapter!

If the interaction happens inside the detector and the energy transfer to the hadronic part of the shower is larger, it will create a cascade with a track leaving it. A similar signature is observed after a ν_τ - CC interaction, in which a tau is produced that later decays into a muon, with a branching ratio of 17 %. In those cases the muon usually has a lower energy and the track will be fainter and harder to observe.

The other 83 % of ν_τ - CC interactions produce a tau that decays into an electron or hadrons, leaving a cascade-only signature through the electromagnetic or hadronic shower. All ν_e - CC interactions also produce pure cascades, since the electron quickly loses its energy in an electromagnetic shower. In all ν - NC interactions, the produced neutrino escapes and only the hadronic shower is observable. Since the size of the cascades at the energy range of interest is smaller than the spacing of the DOMs, they are approximately observed as point-like, spherical light sources. Considering the short effective scattering length (20 m-50 m), the light is almost isotropically emitted.

SB: Since your analysis depends on the ability to reconstruct cascade directions, it seems odd to emphasize that the light is nearly isotropically emitted. Of course that is true, but the emphasis should rather be on the fact that there remains some asymmetry to the light profile

Atmospheric muons also produce pure track like signatures, similar to ν_μ - CC interactions happening outside the detector. They are one of the main backgrounds for analyses using atmospheric neutrinos and are therefore the target of many filter steps described in Section 3.3.1.

Heavy Neutral Lepton Signal Simulation

2

The central part of this thesis is the HNL signal simulation itself. Since this is the first search for HNLs with IceCube DeepCore, there was no prior knowledge of the number of events expected per year nor of the expected performance in terms of reconstruction and classification accuracy which governs the 90 % confidence level on estimateing the $|U_{\tau 4}|^2$ mixing matrix element. This is the first HNL simulation developed for IceCube DeepCore. Two avenues of simulation generation were pursued in parallel. The physically accurate, model dependent simulation is described in Section 2.2 and a collection of model independent simulation samples was realized and is explained in Section 2.1. The latter is used for performance benchmarking and as a cross-check for the model dependent simulation. The SM simulation generation and the default low energy event selection and processing chain are introduced in Chapter 3 and everything but the generation is applied identically to both neutrinos and HNLs.

2.1 Model Independent Simulation

To investigate the potential of IceCube to detect HNLs by identifying the unique double cascade morphology explained in Section ??, it is very valuable to have a simulation chain where the double cascade kinematics can be controlled directly. In a realistic model the decay kinematics and the absolute event expectation all depend on the specific model parameters chosen (see Section ??). To decouple the simulation from a specific parameter choice, a model independent double cascade generator was developed. Using this generator several simulation samples were produced to investigate the performance of IceCube DeepCore to detect low energetic double cascades, dependent on their properties. All samples are produced using a collection of custom generator functions [19] that place two EM cascade vertices with variable energy and direction at choosable locations in the detector. The results of this study will be discussed in Chapter ??.

2.1.1 Simplistic Samples

To investigate some idealistic double cascade event scenarios, two samples are produced for straight up-going events that are centered on a string and horizontal events located inside DeepCore.

The first sample is used to investigate one of the most promising scenarios to detect a double cascade, where both cascade centers are located on a DeepCore string (namely string 81) and the directions are directly up-going. The horizontal positions and distances of all DeepCore fiducial volume strings are shown in Figure 2.1 and string 81 is at a medium distance of ~ 70 m to its neighboring strings. As already mentioned in Section 1.1.3, DeepCore strings have higher quantum efficiency DOMs and a denser vertical spacing, making them better to detect low energetic

2.1 Model Independent Simulation	9
2.2 Model Dependent Simulation	12

Make my own DC string positions/distances plot version, viable for the margin?

Maybe just reference the one from the detector description and drop it here?

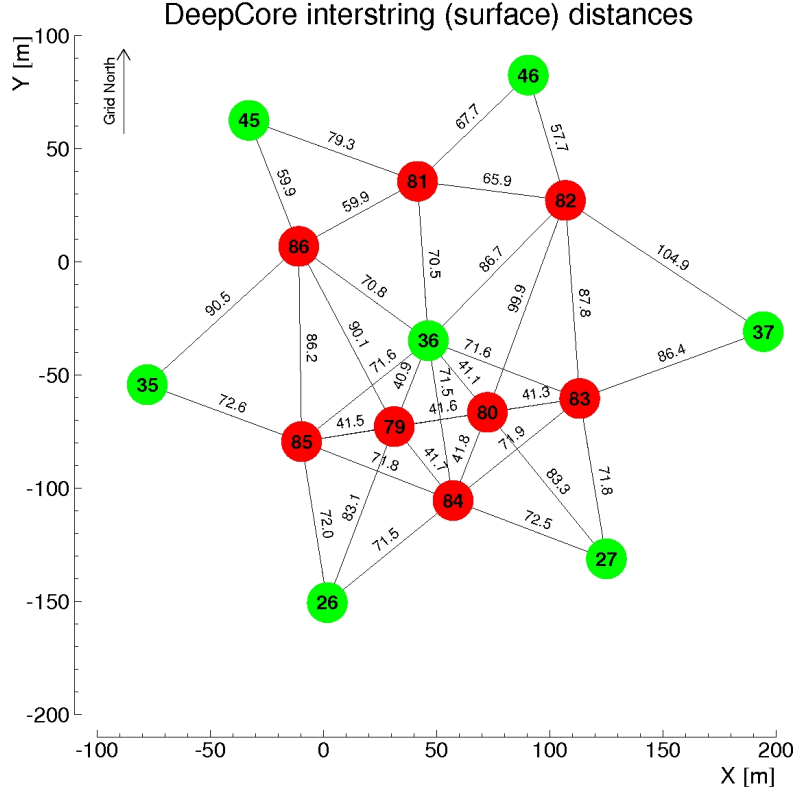


Figure 2.1: Horizontal positions and distances between DeepCore strings. Red strings are instrumented more densely (vertically) and partially have higher quantum efficiency (HQE) DOMs.

events that produce little light. To produce the events, the x, y position of the cascades is fixed to the center of string 81 while the z position is sampled uniformly along the axis of the string. The energies are sampled uniformly between 0.0 GeV and 60.0 GeV. The specific sampling distributions/values for the cascades are listed in Table 2.1. The order of the cascades is chosen such that the lower one is first ($t_0 = 0.0$ ns) and the upper one is second ($t_1 = L/c$), assuming the speed of light c as speed of the heavy mass state, traveling between the two cascades.

The second sample is used to investigate the reconstruction performance for horizontal events, where the spacing between DOMs is much larger. The cascades are placed uniformly on a circle centered in DeepCore. The direction is always horizontal and azimuth is defined by the connecting vector of both cascade positions. The energies are again sampled uniformly between 0.0 GeV and 60.0 GeV and the detailed sampling distributions/values are also listed in Table 2.1. Some examples of the generation level distributions of the simplified samples are shown in Figure 2.2, while further distributions can be found in Figure A.1.

Re-make plot with all energies (cascades and total, both samples (they are the same))

Re-make plot with all decay lengths (both samples)

2.1.2 Realistic Sample

To thoroughly investigate the potential of IceCube DeepCore to detect double cascade events, a more realistic simulation sample is produced that aims to be as close as possible to the expected signal simulation explained in Section 2.2, while still allowing additional freedom to control the double cascade kinematics. For this purpose the total energy is sampled from an E^{-2} power law, mimicking the energy spectrum of the primary neutrinos as stated in Section 3.1.1. The total energy is divided

Sample	Variable	Distribution	Range/Value
Up-going			
	energy	uniform	0.0 GeV to 60.0 GeV
	zenith	fixed	180.0°
	azimuth	fixed	0.0°
	x, y position	fixed	(41.6, 35.49) m
	z position	uniform	-480.0 m to -180.0 m
Horizontal			
	energy	uniform	0.0 GeV to 60.0 GeV
	zenith	fixed	90.0°
	azimuth	uniform	0.0° to 360.0°
	x, y position	uniform (circle)	$c=(46.29, -34.88)$ m, $r=150.0$ m
	z position	fixed	-330.0 m

Table 2.1: Generation level sampling distributions and ranges/values of up-going and horizontal model independent simulation.

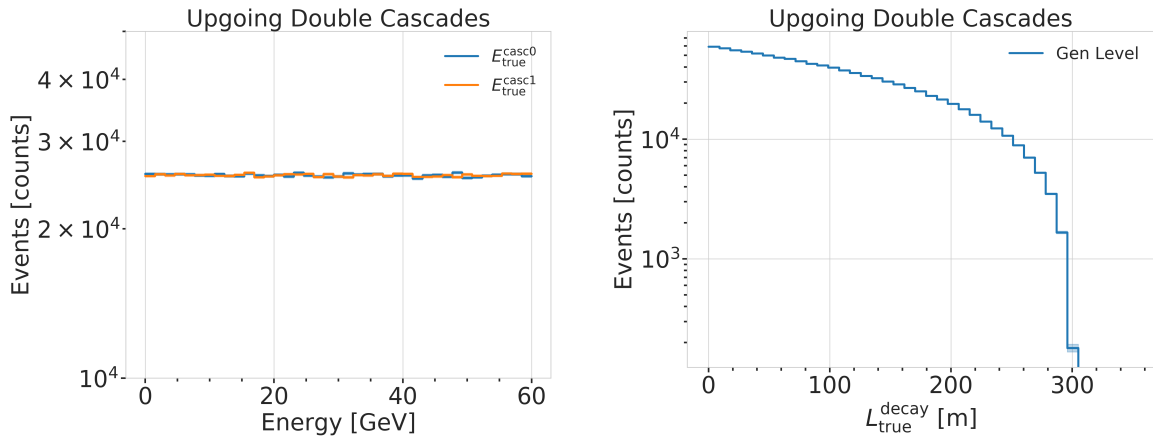


Figure 2.2: Generation level distributions of the simplistic simulation samples. Cascade and total energies (left) and decay lengths (right) of both samples are shown.

into two parts, by randomly assigning a fraction between 0 % and 100 % to one cascade and the remaining part to the other cascade. This is a generic approximation of the realistic process described in Section 2.2, and chosen such that the whole sample covers various cases of energy distributions between the two cascades. To efficiently generate events in a way that produces distributions similar to what would be observed with DeepCore, one of the cascade positions is sampled inside the DeepCore volume by choosing its coordinates randomly on a cylinder that is centered in DeepCore. This is similar to a trigger condition of one cascade always being inside the DeepCore fiducial volume. By choosing the direction of the event by sampling zenith and azimuth uniformly between 70° and 180° and 0° and 360°, respectively, the position of the other cascade can be inferred for a given decay length, assuming a travel speed of c , and randomly choosing whether the cascade position that was sampled is the first cascade or the second. The decay length is sampled from an exponential distribution, as expected for a decaying heavy mass state. The sampling distributions/values are listed in Table 2.4. Example distributions of the generation level variables are shown in Figure 2.3, while further distributions can be found in Figure A.2.

Table 2.2: Generation level sampling distributions and ranges/values of the realistic model independent simulation.

Variable	Distribution	Range/Value
energy (total)	power law E^{-2}	1 GeV to 1000 GeV
decay length	exponential $e^{-0.01L}$	0 m to 1000 m
zenith	uniform	70° to 180°
azimuth	uniform	0° to 360°
x, y (one cascade)	uniform (circle)	$c=(46.29, -34.88)$ m, $r=150$ m
z (one cascade)	uniform	-480.0 m to -180.0 m

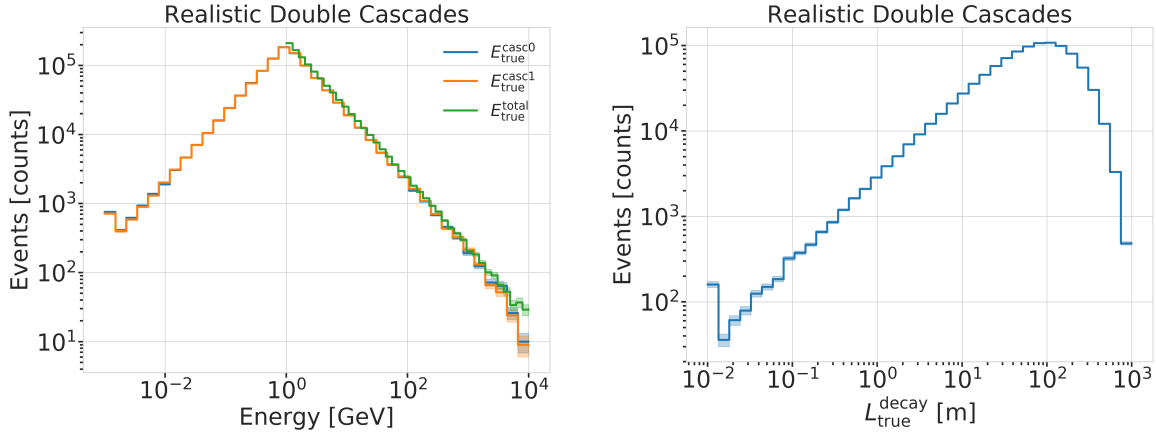


Figure 2.3: Generation level distributions of the simplistic realistic sample. Shown are the cascade and total energies (left) and decay lengths (right).

2.2 Model Dependent Simulation

To estimate the HNL event expectation in IceCube DeepCore, depending on the specific model parameters, a generator was developed that is based on the HNL theory introduced in Section ???. For this work, only the interaction with the τ -sector was taken into account ($|U_{\alpha 4}^2| = 0$, $\alpha = e, \mu$), which reduces the physics parameters of interest and relevant for the simulation to the fourth heavy lepton mass, m_4 , and the mixing, $|U_{\tau 4}^2|$. The generator uses a customized *LeptonInjector* (LI) version to create the events and *LeptonWeighter* (LW) to weight them [20]. The modified LI and the essential components needed for the HNL simulation are described in the next sections, followed by the description of the weighting scheme and the sampling distributions chosen for the simulation generation.

[20]: Abbasi et al. (2021), “LeptonInjector and LeptonWeighter: A neutrino event generator and weighter for neutrino observatories”

2.2.1 Custom LeptonInjector

In its standard version, the LI generator produces neutrino interactions by injecting a lepton and a hadronic cascade at the interaction vertex of the neutrino, where the lepton is the charged (neutral) particle produced in a CC (NC) interaction and the cascade is the hadronic cascade from the breaking nucleus. The hadronic cascade is stored as a specific object of type *Hadrons*, which triggers the correct simulation of the shower development in the following simulation steps, identical to what will be described for SM neutrino simulation on Section 3.1.1. The main differences to an EM cascade is that part of the energy will not be observed, because it goes into neutral particles, and that the spatial

development of the shower is different. Both objects are injected with the same (x, y, z, t) coordinates and the kinematics are sampled from the differential and total cross-sections that are one of the inputs to LI.

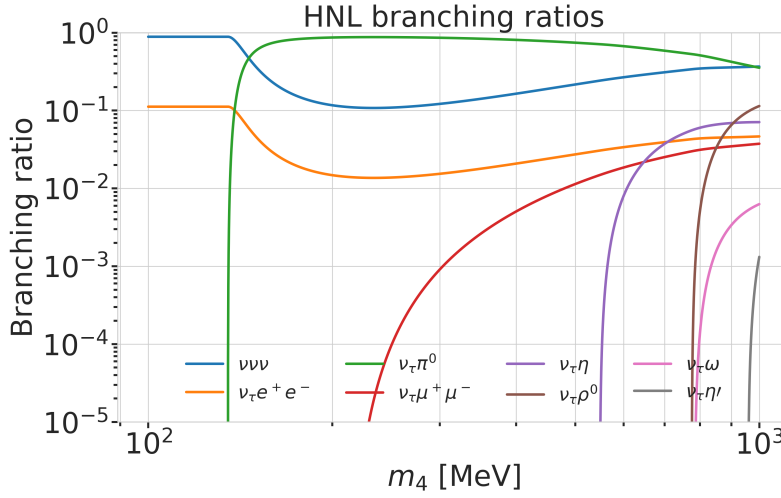


Figure 2.4: Branching ratios of the HNL within the mass range considered in this work, only considering $|U_{\tau 4}^2| \neq 0$, calculated based on the results from [21].

In the modified version, the SM lepton at the interaction vertex is replaced by the new HNL particle, where the interaction cross-sections are replaced by custom, mass dependent HNL cross-sections. The HNL is forced to decay after a chosen distance to produce secondary SM particles, where the decay mode is randomly chosen based on the mass dependent branching ratios from the kinematically accessible decay modes shown in Figure 2.4. The cross-section and decay width calculations were implemented for this purpose and will be explained in more detail in the following. Another needed addition to LI is that the decay products of the HNL are also added to the list of MC particles in each event. They are injected with the correctly displaced position and delayed time from the interaction vertex, given the HNL decay length. These HNL daughter particles form the second cascade, not as a single hadronic cascade object, but as the explicit particles forming the shower. The kinematics of the two-body decays are computed analytically, while the three-body decay kinematics are calculated with MADGRAPH [22], which will also be explained further below. Independent of the number of particles in the final state of the HNL decay, the kinematics are calculated/simulated at rest and then boosted along the HNL momentum.

[22]: Alwall et al. (2014), “The automated computation of tree-level and next-to-leading order differential cross sections, and their matching to parton shower simulations”

The injection is done using the LI *volume mode*, for the injection of the primary particle on a cylindrical volume, adding 50 % of the events with ν_τ and the other half with $\bar{\nu}_\tau$ as primary particle types. The generator takes the custom double-differential/total cross-section splines described below and the parameters defining the sampling distributions as inputs.

Cross-Sections

The cross-sections are calculated using the NuXSSPLMkr [23] software, which is a tool to calculate neutrino cross-sections from *parton distribution functions (PDFs)* and then produce splines that can be read and used with LI/LW. The tool was customized to produce the custom HNL cross-sections, where the main modification to calculate the cross-sections for

In which variables are they splined?

[24]: Levy (2009), “Cross-section and polarization of neutrino-produced tau’s made simple”

the ν_τ -NC interaction into the new heavy mass state is the addition of a kinematic condition to ensure that there is sufficient energy to produce the heavy mass state. It is the same condition fulfilled for the CC case, where the outgoing charged lepton mass is non-zero. Following [24] (equation 7), the condition

$$(1 + x\delta_N)h^2 - (x + \delta_4)h + x\delta_4 \leq 0 \quad (2.1)$$

is implemented for the NC case in the NuXSSplMkr code. Here

$$\delta_4 = \frac{m_4^2}{s - M^2}, \quad (2.2)$$

$$\delta_N = \frac{M^2}{s - M^2}, \text{ and} \quad (2.3)$$

$$h \stackrel{\text{def}}{=} xy + \delta_4, \quad (2.4)$$

with x and y being the Bjorken variables, m_4 and M the mass of the heavy state and the target nucleon, respectively, and s the center of mass energy squared.

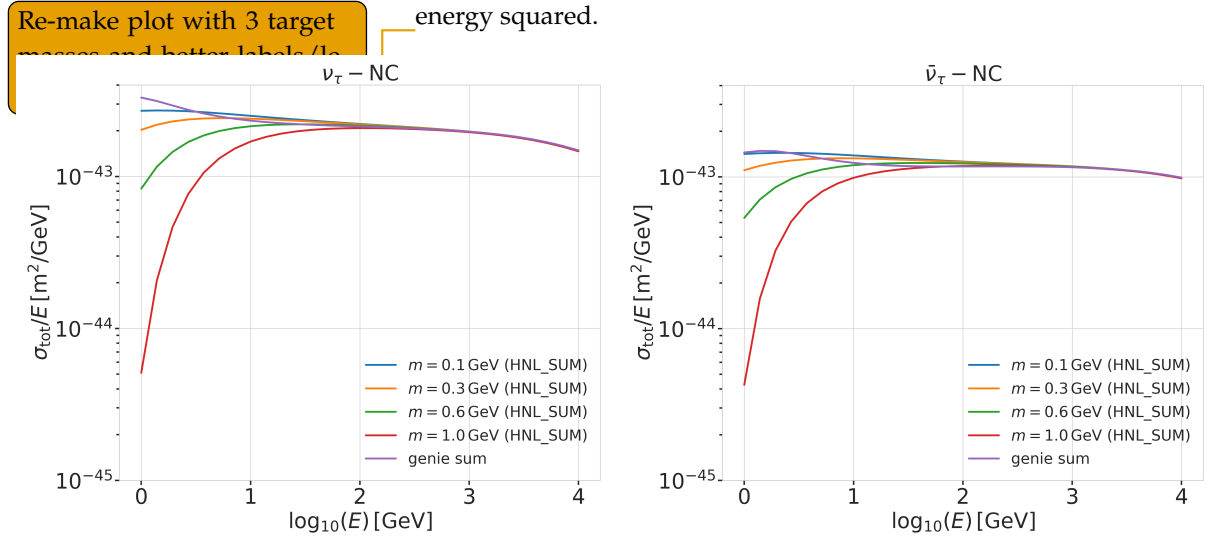


Figure 2.5: Custom HNL total cross-sections for the four target masses compared to the total ($\nu_\tau/\bar{\nu}_\tau$ NC) cross-section used for SM neutrino simulation production with GENIE.

The GRV98LO PDFs were added to the cross-section spline maker and used to create the HNL cross-sections for consistency with the SM neutrino simulation that will be explained in Section 3.1.1. The double differential ($d\sigma/dxdy$) and total (σ) cross-sections were produced for the chosen target HNL masses and then splined. The produced cross-section are added to the custom LI version and used for the simulation generation and weighting. Figure 2.5 shows the total cross-sections that were produced compared to the cross-section used for the production of the SM $\nu_\tau/\bar{\nu}_\tau$ NC background simulation. Above $\sim 2 \times 10^2$ GeV they match, which is the desired result of using the identical input PDFs.

SB: emphasize the cut-off/suppression

Add comparisons of SM cross-sections between NuXSSplMkr and genie?

add varied total cross-section for a few background HNL events (for QE/RES variations?!)

Decay Channels

The accessible decay channels are dependent on the mass of the HNL and the allowed mixing. For this analysis, where only $|U_{\tau 4}|^2 \neq 0$, the decay channels considered are listed in Table 2.3 and the corresponding

branching ratios are shown in Figure 2.4. The individual branching ratio for a specific mass is calculated as $\text{BR}_i(m_4) = \Gamma_i(m_4)/\Gamma_{\text{total}}(m_4)$, where $\Gamma_{\text{total}}(m_4) = \sum \Gamma_i(m_4)$. The individual decay widths Γ_i are computed using the state-of-the-art calculations from [21], which are described in the following.

2-Body Decay Widths The decay to a neutral pseudoscalar meson is

$$\Gamma_{\nu_4 \rightarrow \nu_\tau P} = |U_{\tau 4}|^2 \frac{G_F^2 m_4^3}{32\pi} f_P^2 (1 - x_P^2)^2, \quad (2.5)$$

with $x_P = m_P/m_4$ and the *effective decay constants* f_P given by

$$f_{\pi^0} = +0.1300 \text{ GeV}, \quad (2.6)$$

$$f_\eta = +0.0816 \text{ GeV}, \text{ and} \quad (2.7)$$

$$f_{\eta'} = -0.0946 \text{ GeV}, \quad (2.8)$$

while the decay to a neutral vector meson is given by

$$\Gamma_{\nu_4 \rightarrow \nu_\tau V} = |U_{\tau 4}|^2 \frac{G_F^2 m_4^3}{32\pi} \left(\frac{f_V}{m_V} \right)^2 g_V^2 (1 + 2x_V^2)(1 - x_V^2)^2, \quad (2.9)$$

with $x_V = m_V/m_4$,

$$f_{\rho^0} = 0.171 \text{ GeV}^2, \quad (2.10)$$

$$f_\omega = 0.155 \text{ GeV}^2, \quad (2.11)$$

and

$$g_{\rho^0} = 1 - 2 \sin^2 \theta_w, \quad (2.12)$$

$$g_\omega = \frac{-2 \sin^2 \theta_w}{3}, \quad (2.13)$$

and $\sin^2 \theta_w = 0.2229$ [25].

3-Body Decay Widths The (invisible) decay to three neutrinos is

$$\Gamma_{\nu_4 \rightarrow \nu_\tau \nu_\alpha \bar{\nu}_\alpha} = |U_{\tau 4}|^2 \frac{G_F^2 m_4^5}{192\pi^3}, \quad (2.14)$$

while the decay to two charged leptons (using $x_\alpha = (m_\alpha/m_4)^2$) of the same flavor reads

$$\Gamma_{\nu_4 \rightarrow \nu_\tau l_\alpha^+ l_\alpha^-} = |U_{\tau 4}|^2 \frac{G_F^2 m_4^5}{192\pi^3} [C_1 f_1(x_\alpha) + C_2 f_2(x_\alpha)], \quad (2.15)$$

with the constants defined as

$$C_1 = \frac{1}{4} (1 - 4s_w^2 + 8s_w^4), \quad (2.16)$$

$$C_2 = \frac{1}{2} (-s_w^2 + 2s_w^4), \quad (2.17)$$

the functions as

$$f_1(x_\alpha) = (1 - 14x_\alpha - 2x_\alpha^2 - 12x_\alpha^3)\sqrt{1 - 4x_\alpha} + 12x_\alpha^2(x_\alpha^2 - 1)L(x_\alpha), \quad (2.18)$$

[21]: Coloma et al. (2021), “GeV-scale neutrinos: interactions with mesons and DUNE sensitivity”

Channel	Opens	BR
$\nu_4 \rightarrow \nu_\tau \nu_\alpha \bar{\nu}_\alpha$	0 MeV	1.0
$\nu_4 \rightarrow \nu_\tau e^+ e^-$	1 MeV	?
$\nu_4 \rightarrow \nu_\tau \pi^0$	135 MeV	?
$\nu_4 \rightarrow \nu_\tau \mu^+ \mu^-$	211 MeV	?
$\nu_4 \rightarrow \nu_\tau \eta$	548 MeV	?
$\nu_4 \rightarrow \nu_\tau \rho^0$	770 MeV	?
$\nu_4 \rightarrow \nu_\tau \omega$	783 MeV	?
$\nu_4 \rightarrow \nu_\tau \eta'$	958 MeV	?

Table 2.3: Possible decay channels of the HNL, considering only $|U_{\tau 4}|^2 \neq 0$. Listed is the mass at which each channel opens and the maximum branching ratio.

Calculate max BRs

[25]: Tiesinga et al. (2021), “CODATA recommended values of the fundamental physical constants: 2018”

$$f_2(x_\alpha) = 4[x_\alpha(2 + 10x_\alpha - 12x_\alpha^2)\sqrt{1 - 4x_\alpha} + 6x_\alpha^2(1 - 2x_\alpha + 2x_\alpha^2)L(x_\alpha)] , \quad (2.19)$$

and

$$L(x) = \ln\left(\frac{1 - 3x_\alpha - (1 - x_\alpha)\sqrt{1 - 4x_\alpha}}{x_\alpha(1 + \sqrt{1 - 4x_\alpha})}\right) . \quad (2.20)$$

JVS: consider also writing down the (trivial) 2-body decay kinematics for completeness and consistency.
This transition is a bit jarring as it is

[21]: Coloma et al. (2021), “GeV-scale neutrinos: interactions with mesons and DUNE sensitivity”

3-Body Decay Kinematics with MadGraph

The specific MadGraph version used to produce the 3-body decay kinematics is MadGraph4 v3.4.0. As input, the decay diagrams calculated with FeynRules 2.0 using the Lagrangians derived in [21]. The Universal FeynRules Output (UFO) from `EFFECTIVE_HEAVYN_MAJORANA_v103` were used for our calculation. For each mass and corresponding decay channels, we produce 1×10^6 decay kinematic variations in the rest frame and store those in a text file. During event generation, we uniformly select an event from that list, to simulate the decay kinematics of a 3-body decay.

2.2.2 Sampling Distributions

In principle, the generation level sampling distributions should be chosen such that at final level of the selection chain the phase space relevant for the analysis is covered with sufficient statistics to make a reasonable estimate of the event expectation. Initial distributions insufficiently covering the phase space lead to an underestimate of the expected rates, because part of the events that would pass the selection are not produced. This limits the expected analysis potential. Three discrete simulation samples were produced with HNL masses of 0.3 GeV, 0.6 GeV and 1.0 GeV. Because during development it became clear that the low lengths component is crucial to get a reasonable event estimate, each sample consists of a part that is generated for very short decay lengths and one for long decay lengths. The remaining sampling distributions are identical for all samples and are listed in Table 2.4. The target number of events for each sample was 2.5×10^9 .

Table 2.4: Generation level sampling distributions and ranges/values of the model dependent simulation samples.

Variable	Distribution	Range/Value
energy	E^{-2}	[2 GeV, 1×10^4 GeV]
zenith	uniform (in $\cos(\theta)$)	[80° , 180°]
azimuth	uniform	[0° , 360°]
vertex x, y	uniform	$r=600$ m
vertex z	uniform	-600 m to 0 m
m_4	fixed	[0.3, 0.6, 1.0] GeV
L_{decay}	L^{-1}	[0.0004, 1000] m

2.2.3 Weighting Scheme

1: An analysis in PISA is a collection of functions that are written in so-called *stages*. The stages can be combined in a *pipeline* and are executed in a specific order. This particular stage is located in `pisa/stages/aeff/weight_hnl.py`.

To produce physically correct event distributions based on the simplified generation sampling distributions for the HNL simulation, the forward folding method that was already introduced for the SM simulation in Section 3.1 is also used. The weighting scheme that will be explained

in the following is implemented in a custom stage¹ in the IceCube low energy analysis framework PISA [26], which will be discussed in Section ???. The only required input is the mixing strength $|U_{\tau 4}|^2$, which is the variable physics parameter in this analysis. For each event the gamma factor

$$\gamma = \frac{\sqrt{E_{\text{kin}}^2 + m_4^2}}{m_4}, \quad (2.21)$$

is calculated, with the HNL mass m_4 , and its kinetic energy E_{kin} . The speed of the HNL is calculated as

$$v = c \cdot \sqrt{1 - \frac{1}{\gamma^2}}, \quad (2.22)$$

where c is the speed of light. With these, the lab frame decay length range $[s_{\min}, s_{\max}]$ can be converted into the rest frame lifetime range $[\tau_{\min}, \tau_{\max}]$ for each event

$$\tau_{\min/\max} = \frac{s_{\min/\max}}{v \cdot \gamma}. \quad (2.23)$$

The proper lifetime of each HNL event can be calculated using the total decay width Γ_{total} from Section 2.2.1 and the chosen mixing strength $|U_{\tau 4}|^2$ as

$$\tau_{\text{proper}} = \frac{\hbar}{\Gamma_{\text{total}}(m_4) \cdot |U_{\tau 4}|^2}, \quad (2.24)$$

where \hbar is the reduced Planck constant. Since the decay lengths or lifetimes of the events are sampled from an inverse distribution instead of an exponential, as it would be expected from a particle decay, we have to re-weight accordingly to achieve the correct decay lengths or lifetimes distribution. This is done by using the wanted exponential distribution

$$\text{PDF}_{\text{exp}} = \frac{1}{\tau_{\text{proper}}} \cdot e^{\frac{-\tau}{\tau_{\text{proper}}}}, \quad (2.25)$$

and the inverse distribution that was sampled from

$$\text{PDF}_{\text{inv}} = \frac{1}{\tau \cdot (\ln(\tau_{\max}) - \ln(\tau_{\min}))}. \quad (2.26)$$

This re-weighting factor is then calculated as

$$w_{\text{lifetime}} = \frac{\text{PDF}_{\text{exp}}}{\text{PDF}_{\text{inv}}} = \frac{\Gamma_{\text{total}}(m_4) \cdot |U_{\tau 4}|^2}{\hbar} \cdot \tau \cdot (\ln(\tau_{\max}) - \ln(\tau_{\min})) \cdot e^{\frac{-\tau}{\tau_{\text{proper}}}}. \quad (2.27)$$

Adding another factor of $|U_{\tau 4}|^2$ to account for the mixing at the interaction vertex the total re-weighting factor becomes

$$w_{\text{total}} = |U_{\tau 4}|^2 \cdot w_{\text{lifetime}}. \quad (2.28)$$

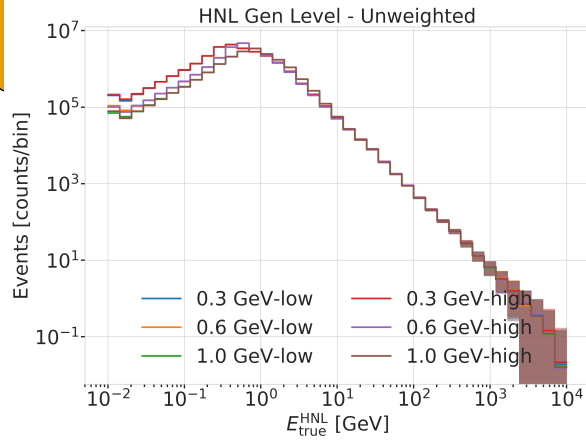
If this additional weighting factor is multiplied to a generation weight with units m^2 (like in Equation 3.1), the livetime in s , and the oscillated primary neutrino flux in $\text{m}^{-2}\text{s}^{-1}$, it results in the number of expected events in the detector for this particular MC event for a chosen mixing (and mass).

add table with number of gen level files? mention the event number is smaller because of kinematic condition?

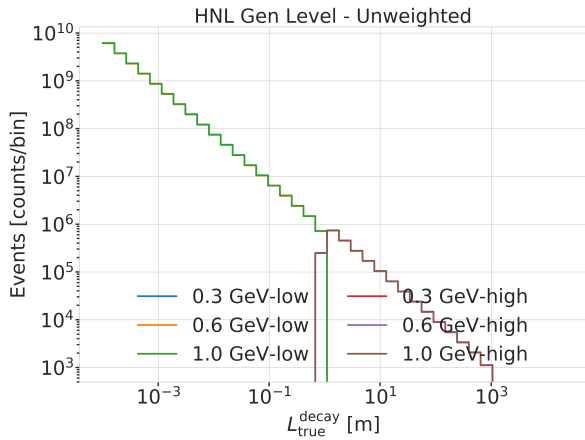
2.2.4 Generation Level Distributions

Figure 2.6 shows some selected generation level distributions. Additional distributions can be found in Figure A.3.

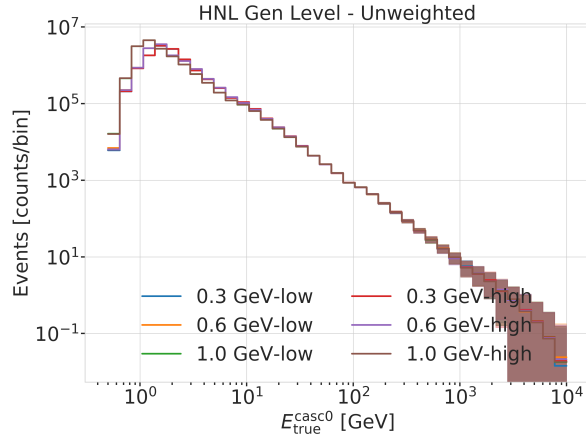
Combine low/high plots
and remove all traces of the



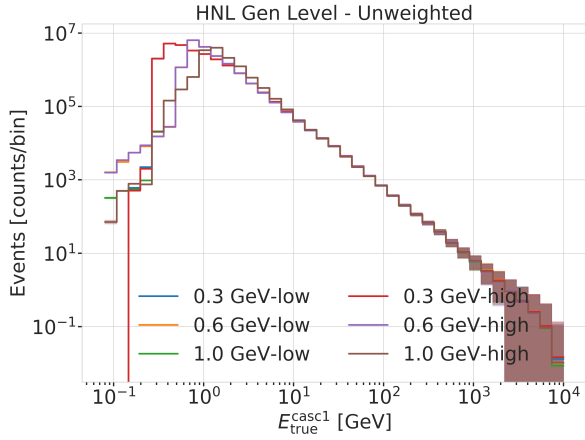
(a) HNL energy



(b) Decay length



(c) First cascade energy



(d) Second cascade energy

Figure 2.6: Generation level distributions of the model dependent simulation.

maybe increase main text width? (read in kao docu)

Adapt to reflect switched chapter order

Standard Model Background Simulation and Data Processing

3

The analysis presented in this thesis is highly dependent on an efficient event selection to reduce the raw IceCube trigger data to a usable atmospheric neutrino sample. Based on this selection, a precise estimation of both expected SM background and expected BSM signal events can be made using MC simulations. This chapter describes the current simulation and event selection chain used for state-of-the-art IceCube neutrino oscillation measurements like [27]. The whole chain can be broadly split into 4 steps:

Step 1 Event Generation: The initial step for all particle (non-noise) simulation is the generation of events from selected initial distributions and fluxes. Events are the primary particle and the particles produced in the interaction with the ice.

Step 2 Detector Simulation: The particles from the first step are propagated through the ice, producing Cherenkov photons, which are then propagated further until they reach a DOM or are absorbed. If they hit a DOM the detector response (acceptance and PMT) is simulated.

Step 3 Processing: Starting from the PMT output, both real data and simulation are processed through the in-ice trigger, the online filter and processing, and the low energy event selection to produce a neutrino dominated sample.

Step 4 Reconstruction: Once the sample is small enough for more sophisticated reconstruction techniques to be feasible to run, the events are reconstructed using a CNN and some high level variables are computed. Based on these variables the final event selection is applied.

This chapter only describes the event generation for the SM background simulation (neutrinos and muons), while the signal simulation is described in Chapter 2. The detector simulation is identical for both signal and background events while processing and reconstruction are applied to all simulation and data in the same way. Splitting the simulation steps has the advantage of reusing the outputs of for example the generation step to propagate the particles with different ice model, in order to estimate the systematic impacts of uncertainties of the ice properties. Similar approach can be taken for varying detector response and through this a more efficient (reduced) use of computing resources can be achieved. The following sections describe the different steps in more detail and the last section, Section 3.5, describes the related systematic uncertainties considered for this work.

3.1 Event Generation

The MC is used in the analysis by applying a method called *forward folding*, where a very large number of events (signal and background) is produced using sampling distribution that are tuned to have a large selection efficiency. Those distributions don't have to be physically correct

3.1	Event Generation	21
3.2	Detector Simulation	23
3.3	Processing	25
3.4	Reconstruction	29
3.5	Systematic Uncertainties	31

[27]: Abbasi et al. (2023), "Measurement of atmospheric neutrino mixing with improved IceCube DeepCore calibration and data processing"

Table 3.1: Cylinder volumes used for GENIE neutrino simulation generation. Cylinder is always centered in DeepCore at $(x, y, z) = (46.29, -34.88, -330.00)$ m.

Flavor	Energy [GeV]	Radius [m]	Length [m]	Events/File	Files
$\nu_e + \bar{\nu}_e$	1-4	250	500	450000	
	4-12				
	12-100	350	600	100000	650
	100-10000	550	1000	57500	
$\nu_\mu + \bar{\nu}_\mu$	1-5	250	500	408000	
	5-80	400	900	440000	
	80-1000	450		57500	1550
	1000-10000	550	1500	6700	
$\nu_\tau + \bar{\nu}_\tau$	1-4	250	500	1500000	
	4-10			300000	
	10-50	350	600	375000	350
	50-1000	450	800	200000	
	1000-10000	550	1500	26000	

distributions, but they need to cover the full parameter space of interest for the analysis. To produce a physical distribution, the events are weighted given a specific choice of physics and nuisance parameters. The large number of raw MC events ensures a good estimation of the expected numbers and weighted distributions.

The analysis itself is then performed by comparing the weighted MC distributions to the observed data. This is done by binning them as described in Chapter ?? and calculating a loss function comparing the bin expectations to the data. The physics and nuisance parameters that best correspond to the observed data are estimated by minimizing this loss function. In order to achieve a reliable result with this method the MC needs to be precise and as close to the data as possible (at least at the final event selection).

3.1.1 Neutrinos

Due to the very low interaction rate of neutrinos, the event generation is performed in a way that forces every event to interact in a chosen sampling volume. The weight of each event is then calculated as the inverse of the simulated neutrino fluence

$$w = \frac{1}{F_{\text{sim}}} \frac{1}{N_{\text{sim}}}, \quad (3.1)$$

where F_{sim} is the number of neutrino events per energy, time, area, and solid angle and N_{sim} is the number of simulated events. If this weight is multiplied by the livetime and the theoretically expected neutrino flux for a given physical model, it results in the number of expected events in the detector for this particular MC event. The baseline neutrino flux used in this thesis, computed for the South Pole, is taken from Honda *et al.* [28].

The simulation volume is a cylinder centered in DeepCore with radius and height chosen such that all events possibly producing a signal are contained. The different sizes, chosen depending on energy and neutrino flavor, are shown in Table 3.1. The directions of the neutrinos are sampled

[28]: Honda et al. (2015), “Atmospheric neutrino flux calculation using the NRLMSISE-00 atmospheric model”

isotropically and the energies are sampled from an E^{-2} power law. The number of simulated events is chosen such that the livetime is more than 70 years for each flavor. Neutrinos and antineutrinos are simulated with ratios of 70% and 30%, respectively.

To simulate the neutrino interaction with the ice, the GENIE event generator [29] (version 2.12.8) is used, resulting in the secondary particles and the kinematic and cross-section parameters. As input, the outdated GRV98LO [30] *parton distribution functions (PDFs)* was used, because it was the only option that could incorporate extrapolations to lower Q^2 [31]. Muons produced in these interactions are propagated using PROPOSAL [32], also simulating their Cherenkov light output. The shower development of gamma rays, electrons, and positrons below 100 MeV and hadronic showers below 30 GeV is simulated using GEANT4 [16] while for higher energies an analytical approximation from [12] is used.

3.1.2 Muons

Atmospheric muons are generated on a cylinder surface enclosing the full IceCube detector array. The cylinder has a height of 1600 m and a radius of 800 m. The energy is sampled from an E^{-3} power law while the other sampling distributions (position, direction) are found from parameterizations based on [33]. This work uses full CORSIKA [34] simulations of muons to tailor the parameterizations, starting from *cosmic ray (CR)* interactions with atmospheric nuclei using the CR flux model from [35] and producing the muons applying the *hadronic interaction (HI)* model SIBYLL 2.1 [36]. After the generation, they are propagated through the ice with PROPOSAL producing photons, treating them exactly like the muons produced in neutrino interactions.

Since the offline processing and selection steps described in Section 3.3.2 and Section 3.4 reduce the muon contamination to an almost negligible level, the statistical uncertainty on the number of expected muon events at the final selection level is large and therefore two separate sets of muon simulation are produced. A **first set** including all events resulting from the above described generation to tune the lower level selection (up to L4) and a **second set** to estimate the muon contamination at higher levels (above L5), which only accepts muon events if they pass through a smaller cylinder centered in DeepCore (height of 400 m and radius of 180 m) and rejects events based on a KDE estimated muon density at L5 (in energy and zenith) increasing the simulation efficiency at L5 significantly.

[29]: Andreopoulos et al. (2015), "The GENIE Neutrino Monte Carlo Generator: Physics and User Manual"

[30]: Glück et al. (1998), "Dynamical parton distributions revisited"

[31]: Bodek et al. (2003), "Higher twist, $\chi(\omega)$ scaling, and effective LO PDFs for lepton scattering in the few GeV region"

[32]: Koehne et al. (2013), "PROPOSAL: A tool for propagation of charged leptons"

[16]: Agostinelli et al. (2003), "Geant4—a simulation toolkit"

[12]: Rädel et al. (2012), "Calculation of the Cherenkov light yield from low energetic secondary particles accompanying high-energy muons in ice and water with Geant4 simulations"

[33]: Becherini et al. (2006), "A parameterisation of single and multiple muons in the deep water or ice"

[34]: Heck et al. (1998), "CORSIKA: A Monte Carlo code to simulate extensive air showers"

[35]: Gaisser (2012), "Spectrum of cosmic-ray nucleons, kaon production, and the atmospheric muon charge ratio"

[36]: Engel et al. (2017), "The hadronic interaction model Sibyll – past, present and future"

put a number on this significant increase?

3.2 Detector Simulation

The detector simulation is performed after the event generation, where the initial particles and the resulting photons and secondary particles from their propagation were produced. This part of the simulation chain is applied to all muon and neutrino simulation as well as the HNL signal simulation explained in detail in Chapter 2. The detector simulation can be split into two parts, the propagation of the photons and the simulation of the detector response (including internal noise).

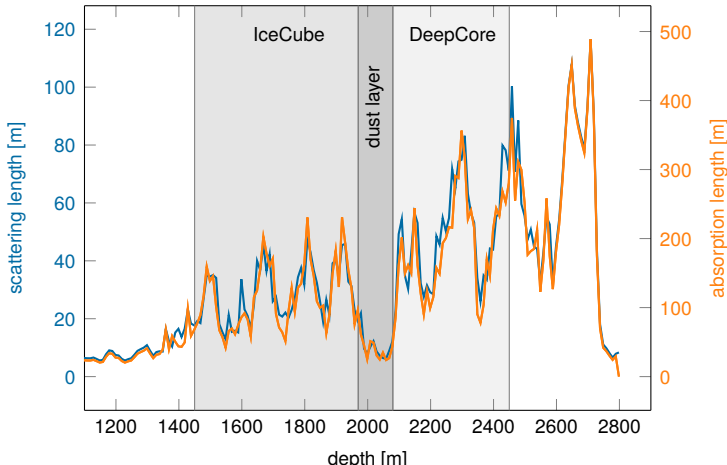


Figure 3.1: Scattering and absorption lengths in the SPICE model used for simulation production as a function of depth, modified from [40].

3.2.1 Photon Propagation

Any photon that was produced in the event generation is individually traced through the ice, simulating scattering and absorption processes. The propagation is done using `CLSIM` [37] which is an implementation of the *Photon Propagation Code (PPC)* [38] in OPENCL. It is optimized to be run very efficiently on GPUs, which is what is done for IceCube simulation production. The ice is modeled as a set of 10 m thick, almost horizontal layers with specific absorption and scattering lengths. The *South Pole ice (SPICE)* model [39] accounts for the layers being tilted by a small amount () and the absorption and scattering lengths having a non-uniformity with respect to the azimuth direction. Figure 3.1 shows the values of this model for the different depths, indicating the location of IceCube, DeepCore, and the dust layer.

In an initial step, each photon's absorption length is sampled from an exponential distribution with the expectation value at the current layer's absorption length. The following propagation steps are performed in parallel for all photons. In each of those steps, corresponding to a single scattering event, the photon travels a length that is sampled from an exponential distribution with the expectation value at the scattering length of the current layer and the scattering angle chosen based on a combination of a simplified Mie scattering distribution [41] and a Henyey-Greenstein distribution [42]. The parameters defining the shape of these distributions were calibrated using data from *in-situ* LED calibration runs. These steps are continuously repeated until each photon reached a DOM or was absorbed¹. After all photons have been propagated in that manner, the final step is to output the photons that reached a DOM for further processing.

3.2.2 Detector Responses

The second part of simulating the IceCube detector is the DOM response. Whether a photon that reached a DOM produces a signal depends on the total efficiency and the angular acceptance curve of the specific DOM. The total efficiency includes effects of the DOM glass, PMT quantum and photo-electron collection efficiencies, and it is wavelength dependent. Additionally, there is another angle dependent effect called *hole ice* [43].

[38]: Chirkin et al. (2019), "Photon Propagation using GPUs by the IceCube Neutrino Observatory"

[39]: Aartsen et al. (2013), "Measurement of South Pole ice transparency with the IceCube LED calibration system"

put a number on the tilt angle?

[41]: Mie (1908), "Beiträge zur Optik trüber Medien, speziell kolloidaler Metallösungen"

[42]: Henyey et al. (1941), "Diffuse radiation in the Galaxy."

1: A photon is absorbed, when it traveled its full absorption length, sampled in the initial step of the photon propagation.

[43]: Fiedlschuster (2019), "The Effect of Hole Ice on the Propagation and Detection of Light in IceCube"

This effect is due to varied ice properties resulting from the re-freezing process of the water column inside the borehole after deployment of the string. Accepted photons are converted into a so-called *Monte Carlo photo-electron (MCPE)*. The amount of charge measured for each MCPE is determined by sampling from a mixture of two exponential distributions and a normal distribution. This *single photo-electron (SPE)* distribution was tuned to match the observed distribution in each DOM in an *in-situ* calibration study [44]. Figure ?? shows the distribution compared to a lab measurement. Based on the sampled charges and times of MCPEs, the voltage waveforms for the (two) different readout channels are simulated and passed on to the trigger simulation starting with *WaveDeform*, which was already mentioned in Section 1.1.1.

Besides the Cherenkov photons, IceCube also observes photons that are produced in radioactive decays inside the DOMs, both in the glass housing sphere and the PMT glass itself. To simulate this internal noise, the *Vuvuzela* module [45, 46] is used to create additional MCPEs that are fed into the same simulation chain described above. This module takes into account thermal and non-thermal components and their times are sampled using parameterizations of the measured distributions, where the thermal noise component is uncorrelated photons and the non-thermal component is from burst of photons. The noise hits are simulated by drawing the times from a constant rate Poisson process and the number of photons from a Poisson distribution. Then the time differences between the individual photons per hit is found, based on a Log-Normal distribution. The simulation is defined by 5 parameters that are calibrated for each DOM individually. Table 3.2 shows the average values for these parameters.

[44]: Aartsen et al. (2020), "In-situ calibration of the single-photoelectron charge response of the IceCube photomultiplier tubes"

Add SPE distribution plot

Parameter	Value
Therm. rate λ_{th}	180 Hz
Decay rate λ_{dec}	80 Hz
Decay hits η	8.5
Decay μ	$4.3 \log_{10}(\text{ns})$
Decay σ	$1.8 \log_{10}(\text{ns})$

Table 3.2: Typical parameter values used in the vuvuzela noise simulation. Averaged over all DOMs.

[45]: Larson (2013), "Simulation and Identification of Non-Poissonian Noise Triggers in the IceCube Neutrino Detector"

[46]: Larson (2018), "A Search for Tau Neutrino Appearance with IceCube-DeepCore"

3.3 Processing

After the detector simulation is performed, all MC and data are processed in exactly the same way. This section explains the trigger and event selection that is applied starting from the raw voltage measured by the PMTs. Most parts of this processing are identical to the procedure already described in [40, 47]. It is split in different steps run inside the ice, at the South Pole, and after the data was transferred to the North. The complexity and computational cost of the processing increases with each step, while the total number of events reduces, making it feasible and reducing the use of computational resources on events that are not of interest for the analysis.

[40]: Trettin (2023), "Search for eV-scale sterile neutrinos with IceCube DeepCore"

[47]: Lohfink (2023), "Testing nonstandard neutrino interaction parameters with IceCube-DeepCore"

3.3.1 Trigger and Filter

Before the data can be sent to the North, the initial signal coming from the PMT (for data) or from the detector response simulation (for MC) is a voltage waveform, which has to be digitized and information of photon hits has to be extracted. The trigger and filter explained here are tailored to select events that passed through the DeepCore volume, while rejecting background events (either from atmospheric muons or from random noise). There are other filters used in IceCube which will not be explained here, since they are not relevant for this work. A full

AT: Das klingt so, als würde die MC Simulation ein analoges Signal erzeugen, was auch digitalisiert wird. Vielleicht kann man das nochmal nachforschen, aber zumindest in meiner Arbeit habe ich geschrieben, dass die MCPEs direkt in ATWD und fADC Readouts umgewandelt werden.

[48]: Aartsen et al. (2017), “The IceCube Neutrino Observatory: Instrumentation and Online Systems”

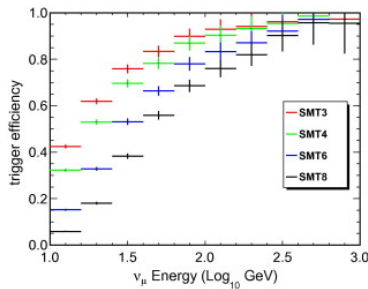


Figure 3.2: Efficiencies of different IceCube and DeepCore triggers, taken from [8].

[4]: Abbasi et al. (2009), “The IceCube data acquisition system: Signal capture, digitization, and timestamping”

[1]: Aartsen et al. (2017), “The IceCube Neutrino Observatory: instrumentation and online systems”

[8]: Abbasi et al. (2012), “The design and performance of IceCube DeepCore”

description of the instrumentation and the online systems can be found in [48].

In-ice Trigger

The trigger is applied inside the DOM in the ice before sending the information to the ICL on the surface. The time dependent voltage curves are captured if a pre-defined threshold value is exceeded. Once the threshold set to the equivalent of 0.25 PE is crossed, 6.4 μ s of the waveform are coarsely digitized by a *Fast Analog-to-Digital Converter (FADC)* with a sampling rate of 40 MHz. Additionally, the first 427 ns are digitized using an *Analog Transient Waveform Recorder (ATWD)* with a sampling rate of 300 MHz [4], but only if some trigger condition is met, because this readout frequency is too high to be sampled directly and requires some buffering. For DeepCore, the HLC condition already mentioned in Section 1.1.1 has to be met for three DOMs inside the fiducial volume within a time window of 5 μ s. If this is the case, all waveforms that crossed the threshold within a 20 μ s time window around the trigger are digitized and sent to the ICL for further processing. This trigger is called *Simple Multiplicity Trigger 3 (SMT-3)*. The DOM hits that are read out in this process, but do not meet the HLC condition, are called *soft local coincidence (SLC)* hits. The rate of the DeepCore SMT-3 trigger is \sim 250 Hz [1], accepting \sim 70 % of ν_μ -CC events at 10 GeV and \sim 90 % at 100 GeV [8]. The trigger efficiencies for different SMT triggers, including the DeepCore SMT-3, are shown in Figure 3.2.

Online Filter

2: Where *online* means running on hardware at the South Pole.

The digitized waveforms are sent to the ICL, where a further filter is applied *online*². First, the WaveDeform algorithm is run to extract photon arrival times and charge from the waveforms, then the DeepCore filter is applied, which is an iterative hit cleaning starting from HLC hits and removing any hits outside a 125 m radius and a 500 ns time window (called *radius-time cleaning (RT-cleaning)*) of the initial hit. This mainly rejects unphysical SLC hits, which are potentially caused by random noise. The following selection steps are done using the resulting cleaned pulses.

Next, an additional cut is applied to reject events that are likely to be caused by atmospheric muons. This is done by splitting the hits depending on whether they were inside the DeepCore fiducial volume or outside and then calculating the speed of each hit outside the fiducial volume towards the *center of gravity (COG)* of the hits inside. If one of them has a speed close to the speed of light, the whole event is rejected, because this is a strong indication for a muon event.

As input for the further selection levels, a few event properties, like vertex position and direction, are determined using fast and simple event reconstructions. After the DeepCore online filter, the rate is about 15 Hz, which can be sent to the North via satellite for further processing.

3.3.2 Event Selection

After the data was sent to the North, the *offline* filters and selection are applied to further reduce the background of atmospheric muons and noise. The selection is split into three levels referred to as *Level 3-5* (*L3-L5*), which bring down the neutrino and muon rate to ~ 1 mHz, while the remaining fraction of random noise is below 1 %.

Level 3

At the first offline filtering level, Level 3, 1D cuts are used to reduce atmospheric muons, pure noise, and coincident muons. These cuts are targeting regions where the data/MC agreement is poor, so that more sophisticated *machine learning* (ML) techniques can be applied at later levels. The cuts are made using 12 control variables, that are inexpensive to compute for the very large sample at this stage. The variables are related to position, time, and overall number of hits in the event.

Pure noise hits, that are temporally uncorrelated, are cleaned by applying a 300 ns sliding window, requiring the containment of more than 2 hits at its maximum. Additionally, an algorithm is run to check whether the hits show some directionality, accepting them only if they do.

To reduce the amount of muons a series of cuts is applied using spatial and temporal information. Events that have more than 9 hits observed above -200 m or the first HLC hit above -120 m are rejected as well as events where the fraction of hits in the first 600 ns of the event is above 0.37, ignoring the first two hit DOMs. Additionally, the ratio between hits in the veto region and the DeepCore fiducial volume is required to be below 1.5.

If a muon enters the detector after the data acquisition was already triggered, it causes events that span over a much larger time range. To reduce those coincident events, the time difference between first and last pulse cannot be above 5000 ns. This cut mainly affects a region of very poor data to MC agreement, because coincident events are not simulated at all.

The L3 cuts remove 95 % of the atmospheric muons and >99 % of pure noise hits, while keeping >60 % of the neutrino events. The sample now roughly contains muons/neutrinos/noise at a ratio of 100:10:1 with a total rate of ~ 0.5 Hz.

add example plots (?) for L3 cut variables and applied cuts

Level 4

After the total rate was reduced by the simple cuts of L3 and the overall agreement between data and MC is established, ML techniques can be applied to further reduce the background. For Level 4, two *Boosted Decision Trees* (BDTs) [49] classifier are trained to separate neutrino events from atmospheric muons and noise hits, separately. The output of each classifier, a probability score, can be seen in Figure 3.3. The noise filter is applied first and an event passes the score if it is larger than 0.7, reducing the noise hits by a factor of 100, while keeping 96 % of neutrinos. Then the second BDT classifier is applied to reject muons. It was trained partly

[49]: Friedman (2002), “Stochastic gradient boosting”

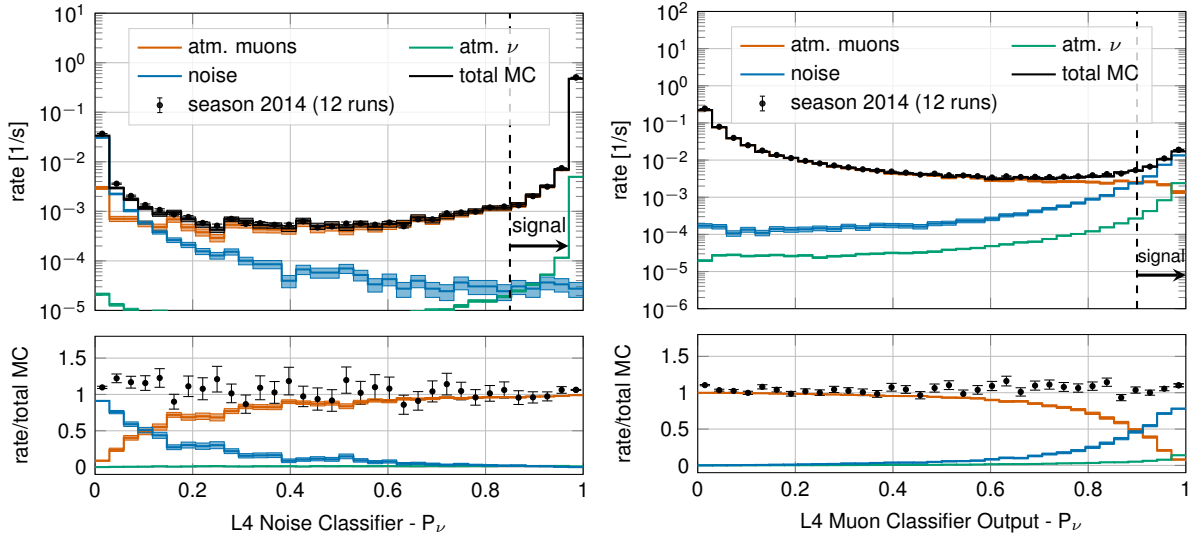


Figure 3.3: Distributions of Level 4 noise classifier output (left) and muon classifier output (right), where larger values indicate more neutrino-like and lower values more noise-like/muon-like. Taken from [27].

on unfiltered data, which consists of >99 % atmospheric muons, to reject the data and keeping the neutrinos from the simulation. Rejecting events with a score smaller than 0.65 removes 94 % of atmospheric muons while keeping 87 % of neutrinos. This fraction varies depending on the flavor and interaction type, ν_μ -CC events for example, which have a muon in the final state, are therefore reduced to 82.5 %. After applying the L4 cuts based on the BDT classifier outputs, the sample is still dominated by atmospheric muons, while the noise rate dropped to below most neutrino types.

Level 5

add some figure showing the corridors?

Level 5 is the final selection level, before event reconstructions are applied. This level aims to reduce the remaining atmospheric muon rate below the rate of neutrinos. Muons not rejected by the earlier levels are those that produced little or no light in the veto regions. One possible reason is that they passed through one of the un-instrumented regions between the strings called *corridors*. To reject those, special corridor cuts, based on the number of hits they produced close to a potential corridor they passed through. The potential corridor in question is identified based on a simple infinite track fit. In addition to the corridor cuts, starting containment cuts are applied to reject events that start at the edge of the fiducial volume. Events with more than seven hits in the outermost strings of the detector or those that have a down going direction in the uppermost region are rejected. This further reduces the fraction of muons by 96 % while keeping 48 % of neutrinos. The rates after this level are 1 mHz and 2 mHz for neutrinos and muons, respectively, making it a neutrino dominated sample.

add table with rates per level (split in flavor) - maybe better in analysis chapter to also show signal?

3.4 Reconstruction

In the energy range most relevant for this work, between 10 GeV and 100 GeV, the light deposition is very low and only a few DOMs detect light, making the reconstructions difficult. In [50] two classical methods are described, which have partly been applied in one recent IceCube atmospheric neutrino oscillation measurement using a sub-sample of the DeepCore sample [27]. The algorithm used in this work on the other hand, is a newer method that applies a *convolutional neural network (CNN)* to reconstruct the events and determine some discriminating quantities. The latest muon neutrino disappearance result from IceCube [51] is based on this reconstruction.

[50]: Abbasi et al. (2022), “Low energy event reconstruction in IceCube DeepCore”

[27]: Abbasi et al. (2023), “Measurement of atmospheric neutrino mixing with improved IceCube DeepCore calibration and data processing”

[51]: Yu et al. (2023), “Recent neutrino oscillation result with the IceCube experiment”

3.4.1 Fast Low Energy Reconstruction using Convolutional Neural Networks

As the name *Fast Low Energy Reconstruction using Convolutional Neural Networks (FLERCNN)* already indicates, the FLERCNN reconstruction [52, 53] is a CNN optimized to reconstruct IceCube events at low energies (<100 GeV) in a fast and efficient manner, by leveraging the approximate translational invariance of event patterns within the detector. The architecture of the network is very similar to the preexisting IceCube CNN event reconstruction [54], but optimized on low energy events and specifically tailored to include the DeepCore sub-array. Only the eight DeepCore strings and the central 19 IceCube strings are used for the reconstruction (compare to Figure 1.4). Because of the different z-positions of the DeepCore and IceCube DOMs, they are divided into two networks that are combined in the final layer of the network. The full architecture is shown in Figure 3.4. The first dimension of the network is the string index, while the second dimension is the order of the DOMs along the vertical axis. The horizontal position of the DOMs is not used, since the strings are arranged in an irregular pattern. The information from the DOM hits is summarized into five charge and time variables, which make up the last dimension of the input layer. The variables are the total summed charge, the time of the first hit, the charge weighted mean time of the hits, the time of the last hit, and the charge weighted standard deviation of the hit times.

[52]: Yu et al. (2021), “Direction reconstruction using a CNN for GeV-scale neutrinos in IceCube”

[53]: Micallef ()

[54]: Huenefeld (2017), “Deep Learning in Physics exemplified by the Reconstruction of Muon-Neutrino Events in IceCube”

Five different networks are trained using this architecture. Three networks do the regression of the events’ energy, zenith angle, and the starting vertex (x, y, z position), while two of them are used for classification. One is trained to predict the probability of the event being a track (used as PID) and the other to predict the probability of the event being a muon. Each network is trained with an MC sample modified to have a flat distribution in the target variable, to be unbiased for that variable and ideally extending outside the target reconstruction region. For the classification tasks the loss function is the *binary cross entropy* and the activation function is a *sigmoid*. To perform the regression of zenith and vertex position, the loss function is the *mean squared error (MSE)*, while for the energy it is the *mean absolute percentage error*. The activation for all regression tasks is *linear*.

add image with selected strings used for flercnn IC and DC

add some performance plots of the FLERCNN reconstruction

There is more information on pre-processing the samples and preparing the input features, and training each cnn, but I’m not sure if that might be too much detail?

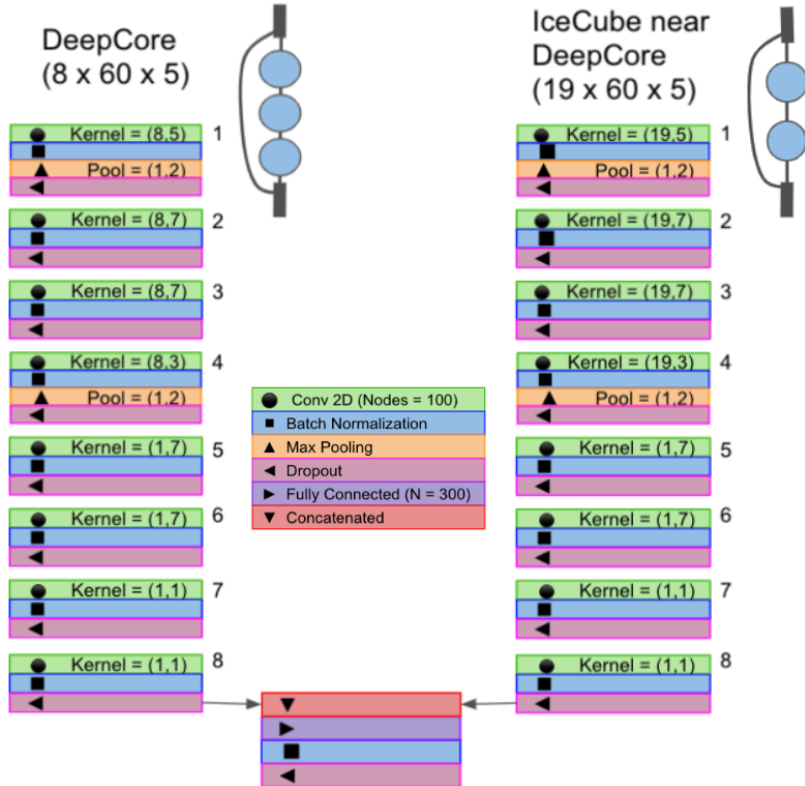


Figure 3.4: Architecture of the FLERCNN neural networks, taken from [52].

3.4.2 Analysis Selection

Before the reconstruction is applied a few additional high level variables are computed, which are from fast and inexpensive algorithms. Then the reconstruction is performed by applying the trained FLERCNN networks to get the output quantities. After that, another BDT classifier is trained to further reduce the muon background for the final sample. The BDT is trained on five high level variables, where three are FLERCNN reconstruction variables (vertex z , ρ_{36}^3 , and muon probability) and two are lower level variables (L4 muon classifier output and L5 corridor cut variable). To train the BDT, the FLERCNN nominal simulation set is used, only using events with $\cos(\theta_{\text{zenith}}) \leq 0.3$. The output of the BDT is the neutrino probability and a cut at 0.8 is applied to reject events with a high probability of being a muon. Figure 3.5 shows the output of the BDT classifier, where the neutrinos in both training and testing sets are gathered at 1 and muons are around 0, which shows great classification power.

To get the final, pure sample of well reconstructed neutrinos another set of cuts is applied. The first cuts are meant to reject events with poor reconstruction quality, by requiring the events to fall into the DeepCore volume, where the denser, better instrumented detector leads to enhanced resolution. The cuts are applied on the vertex z and ρ_{36} and are listed in Table 3.3. The FLERCNN reconstruction was optimized for atmospheric neutrino analyses which are mainly in the region below 100 GeV and there are very few events with energies below 5 GeV, so the reconstructed energy is required to be in that range. Additionally, rejecting events with fewer than seven hits in the selected DOMs used for FLERCNN showed to increase the resolution.

add reference for flercnn analysis internal note

3: A radial variable that is often used in IceCube, is the horizontal distance to string 36 called ρ_{36} , which is basically the distance to the center of IceCube.

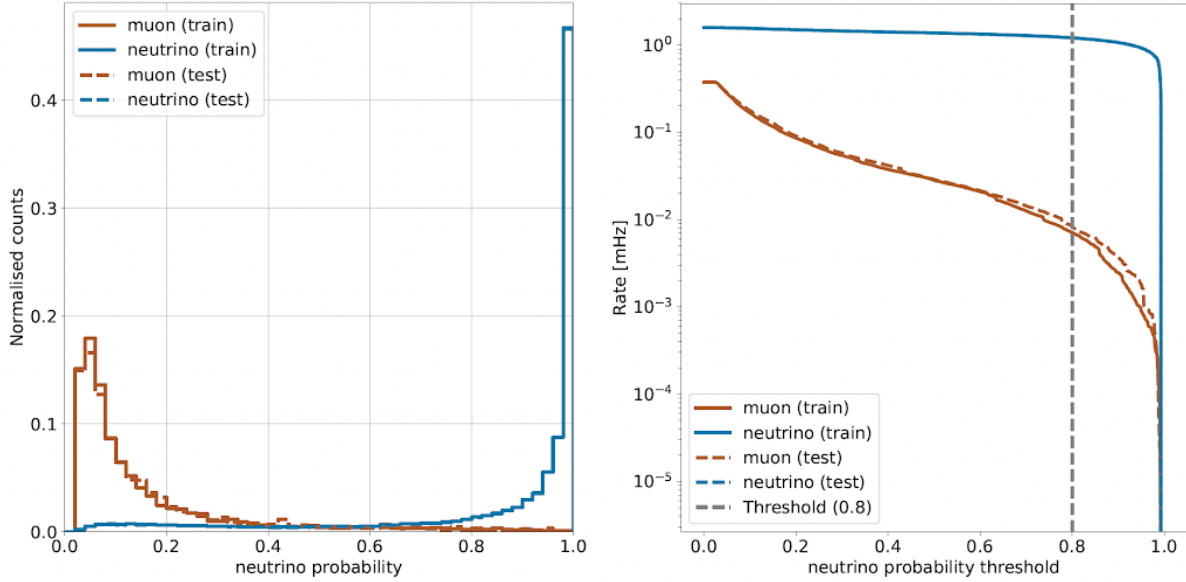


Figure 3.5: FLERCNN muon classifier output score (left) and rate of neutrinos and muons as function of muon classifier cut (right). Taken from [\[flercnn_analysis_internal_note\]](#)

Variable	Threshold	Removed
Number of hit DOMs	≥ 7	1.05 %
Radial distance	$< 200 \text{ m}$	0.09 %
Vertical position	$-495 \text{ m} < z < -225 \text{ m}$	5.48 %
Energy	$5 \text{ GeV} < E < 100 \text{ GeV}$	20.70 %
Cosine of zenith angle	< 0.04	19.66 %
Number of direct hits	> 2.5	10.50 %
Number of hits in top layers	< 0.5	0.03 %
Number of hits in outer layer	< 7.5	0.001 %
Muon classifier score	≥ 0.8	23.90 %

Table 3.3: Cuts performed to select the final analysis sample. Parts of the cuts are meant to increase the data/MC agreement, while others are meant to reject events with poor reconstruction quality.

Another set of cuts is applied to make sure the agreement between data and MC is good. To remove coincident muon and neutrino events, cuts are applied to the number of hits in the top 15 layers of IceCube DOMs and the number of hits in the outermost IceCube strings. Coincident random noise events are removed by requiring more than three hit DOMs from direct photons⁴. Neither of the two coincident event types are simulated, which can be seen as bad agreement between data and MC. The last cut is on the reconstructed cosine zenith, which is required to be smaller than 0.04 to reject down-going muons.

4: Direct photons are photons that were not scattered on their way from the interaction vertex to the DOM.

add final sample composition, but maybe also in analysis chapter to show signal and background?

at some place I will want a selection efficiency plot for SM BG and HNL signal, but I'm not sure where to put it yet

3.5 Systematic Uncertainties

There are multiple sources of systematic uncertainties related to the event generation and processing explained in this chapter. All uncertainties considered in this work are implemented with parameters that can be varied continuously so that a simultaneous fit of the physics and systematic parameters can be performed. Where possible, a correct model of the effect is used, but in many cases the variations are captured by effective parameters. Uncertainties that solely scale the total event rate are not included individually, since the analysis only uses the relative

distribution of events. A single scaling parameter A_{eff} is used to scale the total neutrino rate instead.

3.5.1 Atmospheric Flux Uncertainties

The flux of atmospheric neutrinos is influenced by multiple factors, the spectrum and composition of CRs, the assumed atmospheric conditions, and the HI model used to describe the air showers development. Uncertainties of the neutrino flux are therefore dictated by the uncertainties on these components, where the variations in atmospheric conditions were found to have negligible effect [27].

[27]: Abbasi et al. (2023), "Measurement of atmospheric neutrino mixing with improved IceCube DeepCore calibration and data processing"

[55]: Dembinski et al. (2017), "Data-driven model of the cosmic-ray flux and mass composition from 10 GeV to 10^{11} GeV"

[56]: Barr et al. (2006), "Uncertainties in atmospheric neutrino fluxes"

[57]: Evans et al. (2017), "Uncertainties in atmospheric muon-neutrino fluxes arising from cosmic-ray primaries"

[27]: Abbasi et al. (2023), "Measurement of atmospheric neutrino mixing with improved IceCube DeepCore calibration and data processing"

[59]: Barr et al. (2006), "Uncertainties in Atmospheric Neutrino Fluxes"

add figure with Barr blocks?

[60]: Riehn et al. (2020), "Hadronic interaction model sibyll 2.3d and extensive air showers"

[55]: Dembinski et al. (2017), "Data-driven model of the cosmic-ray flux and mass composition from 10 GeV to 10^{11} GeV"

5: The choice of flux and HI model have minor impact on the variations.

Cosmic ray flux: The selected sample of atmospheric neutrinos lies around energies of up to 100 GeV. The initial primary particles in the CR flux can have 100 times larger energies and therefore the CR flux between 10 GeV and 10 TeV is important, which dominantly consists of hydrogen and helium nuclei [55]. The uncertainty in this CR flux component can be described as a power law correction [56, 57]

$$\Phi'_\nu = \Phi_\nu \left(\frac{E}{E^*} \right)^{\Delta\gamma}, \quad (3.2)$$

where E^* is the pivot energy and $\Delta\gamma$ is the correction to the power law exponent. This modification propagates into the neutrino flux, which is therefore corrected in the same way. E^* was chosen to be 24 GeV as to minimize the dependence of the overall flux scale on $\Delta\gamma$ [27].

Hadronic interaction model: Neutrinos are produced in the decaying hadrons in CR air showers, spanning a large parameter space that is sparsely evaluated by experimental data. To include uncertainties based on energy, direction, and neutrino flavor, the MCEq package [58] is used to compute the distribution of atmospheric leptons and to estimate the impact of varying their contributions. The calculations result in the change in flux $d\Phi_1/dB$ for a variation dB of some parameter B . Scaling this variation by some value b , the modified total flux, s is then given by

$$\Phi'_1 = \Phi_1 + \left(b \cdot \frac{d\Phi_1}{dB} \right). \quad (3.3)$$

Matching the work in [59], the parameter space is divided in regions of the primary energy E_i and the energy fraction of the secondary meson x_{lab} , with varying uncertainties, derived from fixed target experiment data. The Sibyll2.3c [60] HI model and the GSF CR flux [55] were used to calculate the related flux changes⁵ for the different regions in E_i and x_{lab} , resulting in 17 variables, encoding the possible changes.

3.5.2 Cross-Section Uncertainties

The uncertainties related to the cross-sections are split into low and high energy components, since there is no coherent model to explain both DIS interactions, which are the dominant processes above 20 GeV, and *charged current resonance production* (CCRES) and *charged current*

quasi elastic scattering CCQE, which are relevant below 20 GeV where interactions with the nucleons as a whole are important. Three parameters are included to account for all relevant cross-sections uncertainties.

At low energies two parameters are included accounting for uncertainties in form factors of CCQE and CCRES events. These uncertainties are due to uncertainties in the *axial mass* M_A , which enters the form factor as in

$$F(Q^2) \sim \frac{1}{(1 - (\frac{Q}{M_A})^2)^2}, \quad (3.4)$$

where Q^2 is the momentum transfer squared. The axial mass can be determined experimentally and to include uncertainties on the values of M_A^{CCQE} and M_A^{CCRES} , the cross-sections are computed with GENIE, where the form factors are calculated varying the axial mass by $\pm 20\%(1\sigma)/\pm 40\%(1\sigma)$ around the nominal value. This is an approximation of the recommended uncertainties by the GENIE collaboration, which are -15% , $+25\%$ for M_A^{CCQE} and $\pm 20\%$ for M_A^{CCRES} [29]. To apply a continuous uncertainty variation of the axial mass in a fit, the total cross-section is fit with a quadratic function to interpolate between the cross-sections computed with the different axial masses.

which experiments measure the axial mass?

Even though the DIS interactions can be calculated very precisely, there are still uncertainties in the input PDF, describing the probability of finding a specific parton (quark) with a specific momentum fraction x inside a nucleon. To account for differences between the used method and more sophisticated methods using newer PDFs seen at high energies, an uncertainty parameter is introduced. The parameter is based on the discrepancy between the cross-sections computed with GENIE and the ones computed with CSMS [61] above 100 GeV. The included parameter scales the cross-section from the GENIE values to the CSMS values, which are considered more accurate above 100 GeV. The scaling is done as a function of energy and inelasticity and to guarantee continuity, the scaling is extrapolated linearly below 100 GeV. The parameter is designed such that a value of 0.0 corresponds to the GENIE cross-sections and a value of 1.0 gives an approximation of the CSMS cross-sections. A comparison of the total cross-sections GENIE (scaled/unscaled) with the data is shown in Figure 3.6.

[61]: Cooper-Sarkar et al. (2011), “The high energy neutrino cross-section in the Standard Model and its uncertainty”

3.5.3 Detector Calibration Uncertainties

There are multiple sources of systematic uncertainties related to the detection process of neutrinos in IceCube. Dominant for this analysis are the effects of the properties of the ice itself and the optical efficiency of the DOMs. None of these uncertainties can be described by an analytic expression, so they have to be estimated using MC simulation. The method used to derive the continuous variations based on the MC simulation is described in Section ???. The five relevant uncertainty parameters are the absolute efficiency of the DOMs, a global scaling of bulk ice scattering and absorption lengths, and variations of the relative angular acceptance due to hole ice variations in two parameters.

DOM efficiency: As was already mentioned in Section 1.1.1, the absolute efficiency of the DOMs, ϵ_{DOM} is calibrated using minimum ionizing

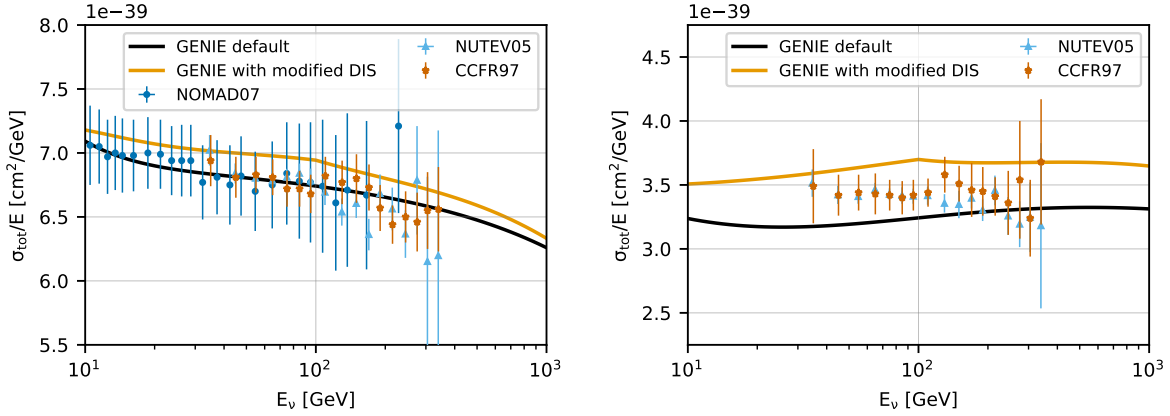


Figure 3.6: Inclusive total neutrino-nucleon cross-sections on an isoscalar target (black) for neutrinos (left) and antineutrinos (right) calculated with GENIE, comparing to measurements from NOMAD [62], NUTEV [63], and CCFR [64]. The scaled GENIE cross-section (orange) is also shown. Taken from [27].

[6]: Feintzeig (2014), “Searches for Point-like Sources of Astrophysical Neutrinos with the IceCube Neutrino Observatory”
[7]: Kulacz (2019), “In Situ Measurement of the IceCube DOM Efficiency Factor Using Atmospheric Minimum Ionizing Muons”

muons from air showers, due to the lack of a calibrated light source in the detector. Using the muons as a steady, controlled source of light, the efficiency can be estimated by comparing simulated muon data sets with varied DOM response to the measured data. Since the uncertainties found in multiple iterations of this study [6, 7] are at the order of 10 %, this systematic is highly relevant and has to be included in the analysis.

Bulk ice scattering and absorption: Absorption and scattering length are the most important properties that govern the propagation of photons through the ice. The simulation principle and how the depth dependent absorption and scattering coefficients are used was already explained in Section 3.2.1. To account for uncertainties on this model of the bulk ice coefficients, a global scaling for each of the two parameters (global absorption, global scattering) is applied.

[65]: Rongen, Martin (2016), “Measuring the optical properties of IceCube drill holes”

6: The hole ice angular acceptance modification is normalized so that it does not affect the total charge.

Hole ice angular acceptance: Due to bubble formation in the re-freezing process of the boreholes, the hole ice seems to be less transparent in the center of the columns [65]. This effectively decreases the chance of photons hitting the DOMs directly from below, which can be described as an additional angular modification of the DOM acceptance. The modification is parameterized by a two dimensional, normalized⁶ function, where the two dominant of the parameters (p_0, p_1), dictating its form, are enough to describe all past and the current hole ice models from both *in-situ* and laboratory measurements. Figure 3.7 shows the acceptance modification as a function of the incident photon angle $\cos(\eta)$. The current baseline model, the variations achieved through modifying p_0 and p_1 , and a laboratory measurement can be seen.

3.5.4 Muon Uncertainties

The muon fraction in the final level selection (see Section 3.4.2) is below 1 %, therefore additional muon systematic uncertainties apart from the spectral index are not implemented, but rather a total muon scaling parameter is added. This total scale is somewhat degenerate with the

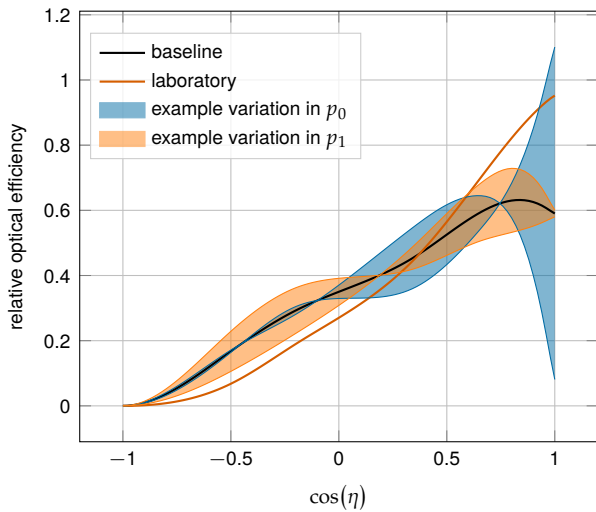


Figure 3.7: Relative angular acceptance modification due to hole ice. Shown is the current baseline model, the variations from changing p_0 and p_1 , and a laboratory measurement. Modified from [40].

DOM efficiency, since an increased DOM efficiency leads to better muon rejection. Both the total muon scaling and the muon spectral index have a very small impact on the analysis as will be shown in Section ??.

cite this?

APPENDIX

A

Heavy Neutral Lepton Signal Simulation

A.1 Model Independent Simulation Distributions

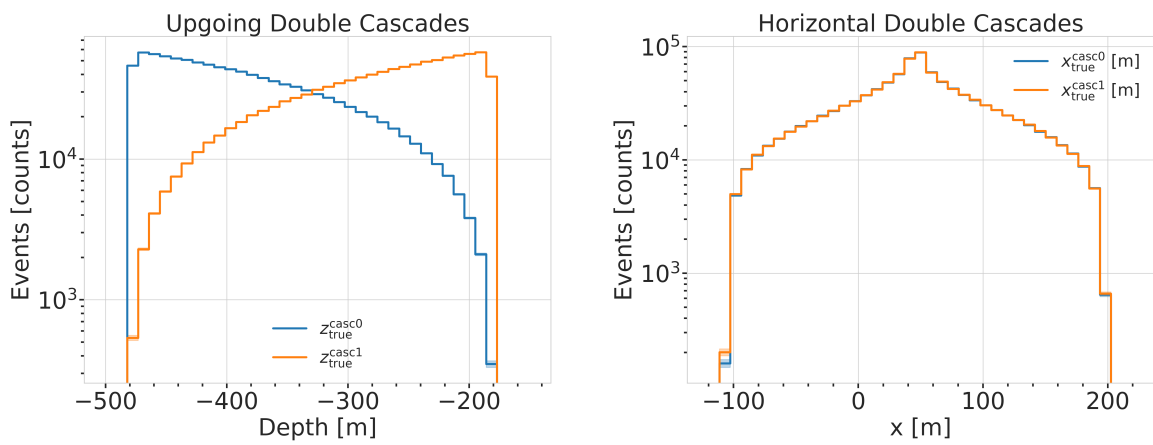


Figure A.1: Generation level distributions of the simplistic simulation sets. Vertical positions (left) and horizontal positions (right) of both sets are shown.

- Re-make plot with x,y for horizontal set one plot!
- Re-make plot with x, y, z for both cascades in one.
- Re-arrange plots in a more sensible way.

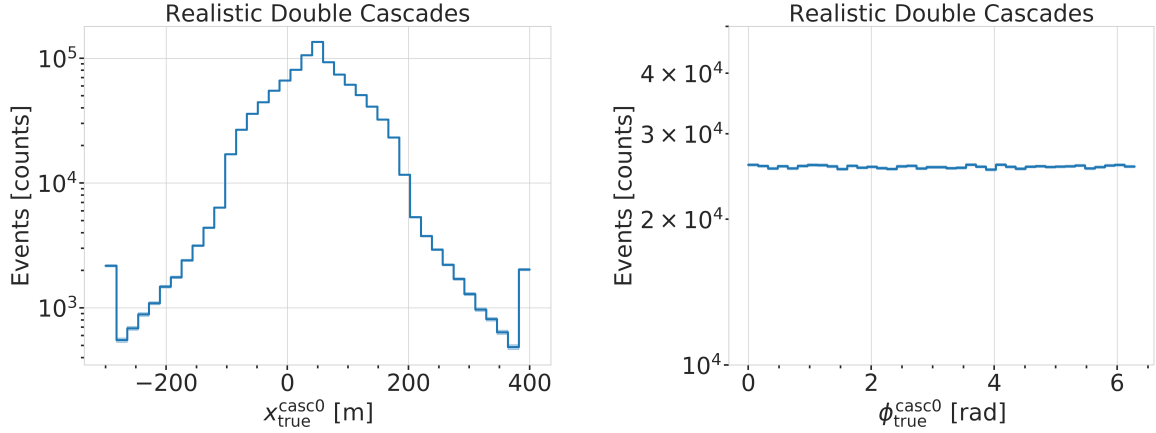


Figure A.2: Generation level distributions of the realistic simulation set. Shown are the cascade x, y, z positions (left) and direction angles (right).

A.2 Model Dependent Simulation Distributions

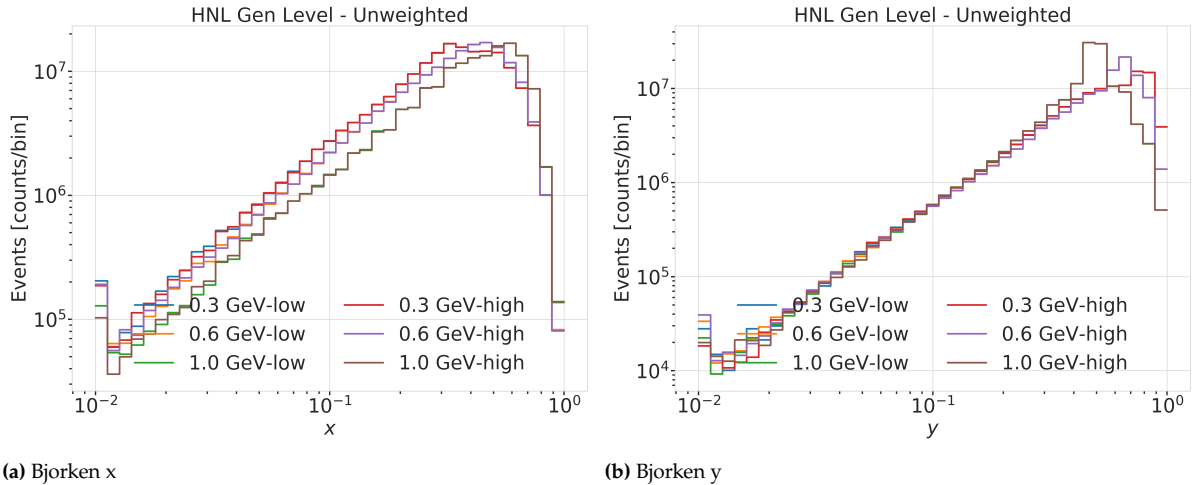


Figure A.3: Generation level distributions of the model dependent simulation.

B

Analysis Checks

B.1 Minimization Robustness

Figure B.1 shows additional Asimov inject/recover tests for the 0.3 GeV and the 1.0 GeV mass sets. The tests were described in Section ??.

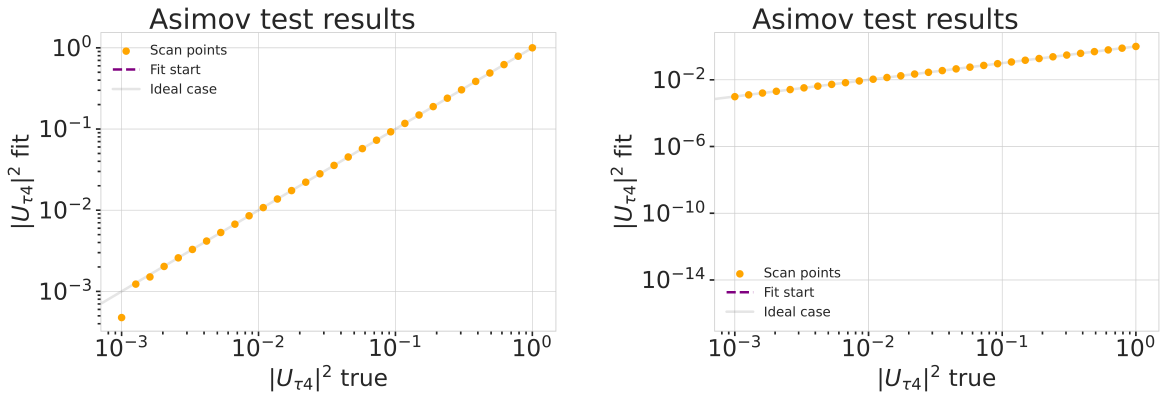


Figure B.1: Asimov inject/recover test for the 0.3 GeV (left) and the 1.0 GeV (right) mass sets. Mixing values between 10^{-3} and 10^0 are injected and fit back with the full analysis chain. The injected parameter is always recovered within the statistical uncertainty.

B.1.1 Ensemble Tests

Figure B.2 shows additional TS distributions from pseudo-data trials and the observed TS from the fit to the data for the ensemble for the 0.3 GeV and the 1.0 GeV mass sets. The tests were described in Section ??.

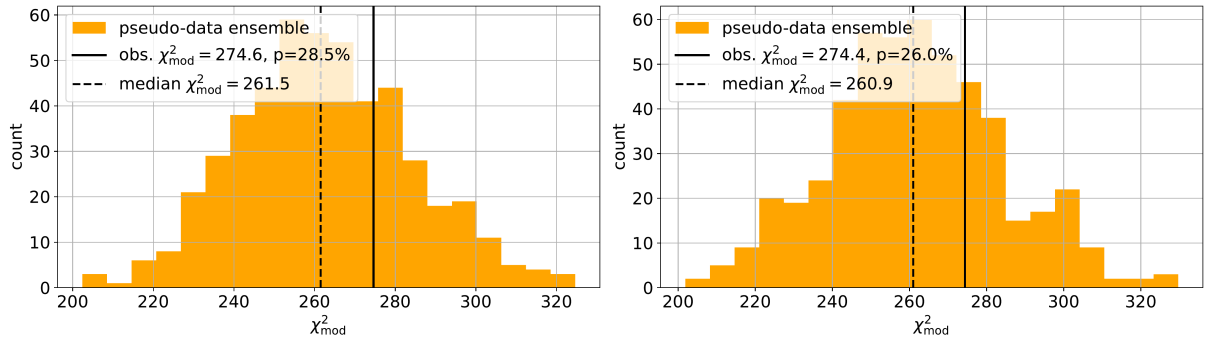


Figure B.2: Observed fit TS and TS distribution from pseudo-data trials for the 0.3 GeV (left) and the 1.0 GeV (right) mass set.

Bibliography

Here are the references in citation order.

- [1] M. G. Aartsen et al. "The IceCube Neutrino Observatory: instrumentation and online systems". In: *Journal of Instrumentation* 12.3 (Mar. 2017), P03012. doi: [10.1088/1748-0221/12/03/P03012](https://doi.org/10.1088/1748-0221/12/03/P03012) (cited on pages 1, 3, 26).
- [2] P. B. Price, K. Woschnagg, and D. Chirkin. "Age vs depth of glacial ice at South Pole". In: *Geophysical Research Letters* 27.14 (2000), pp. 2129–2132. doi: <https://doi.org/10.1029/2000GL011351> (cited on page 2).
- [3] R. Abbasi et al. "In-situ estimation of ice crystal properties at the South Pole using LED calibration data from the IceCube Neutrino Observatory". In: *The Cryosphere Discussions* 2022 (2022), pp. 1–48. doi: [10.5194/tc-2022-174](https://doi.org/10.5194/tc-2022-174) (cited on page 2).
- [4] R. Abbasi et al. "The IceCube data acquisition system: Signal capture, digitization, and timestamping". In: *Nuclear Instruments and Methods in Physics Research Section A: Accelerators, Spectrometers, Detectors and Associated Equipment* 601.3 (2009), pp. 294–316. doi: <https://doi.org/10.1016/j.nima.2009.01.001> (cited on pages 2, 3, 26).
- [5] M. G. Aartsen et al. "Energy Reconstruction Methods in the IceCube Neutrino Telescope". In: *JINST* 9 (2014), P03009. doi: [10.1088/1748-0221/9/03/P03009](https://doi.org/10.1088/1748-0221/9/03/P03009) (cited on page 3).
- [6] J. Feintzeig. "Searches for Point-like Sources of Astrophysical Neutrinos with the IceCube Neutrino Observatory". PhD thesis. University of Wisconsin, Madison, Jan. 2014 (cited on pages 3, 34).
- [7] N. Kulacz. "In Situ Measurement of the IceCube DOM Efficiency Factor Using Atmospheric Minimum Ionizing Muons". MA thesis. University of Alberta, 2019 (cited on pages 3, 34).
- [8] R. Abbasi et al. "The design and performance of IceCube DeepCore". In: *Astropart. Phys.* 35.10 (2012), pp. 615–624. doi: [10.1016/j.astropartphys.2012.01.004](https://doi.org/10.1016/j.astropartphys.2012.01.004) (cited on pages 3, 26).
- [9] P. A. Cherenkov. "Visible Radiation Produced by Electrons Moving in a Medium with Velocities Exceeding that of Light". In: *Phys. Rev.* 52 (4 Aug. 1937), pp. 378–379. doi: [10.1103/PhysRev.52.378](https://doi.org/10.1103/PhysRev.52.378) (cited on page 4).
- [10] I. Frank and I. Tamm. "Coherent visible radiation from fast electrons passing through matter". In: *C. R. Acad. Sci. USSR* 14 (1937), pp. 109–114 (cited on page 5).
- [11] I. Tamm. "Radiation Emitted by Uniformly Moving Electrons". In: *Selected Papers*. Ed. by B. M. Bolotovskii, V. Y. Frenkel, and R. Peierls. Berlin, Heidelberg: Springer Berlin Heidelberg, 1991, pp. 37–53. doi: [10.1007/978-3-642-74626-0_3](https://doi.org/10.1007/978-3-642-74626-0_3) (cited on page 5).
- [12] L. Rädel and C. Wiebusch. "Calculation of the Cherenkov light yield from low energetic secondary particles accompanying high-energy muons in ice and water with Geant4 simulations". In: *Astroparticle Physics* 38 (Oct. 2012), pp. 53–67. doi: [10.1016/j.astropartphys.2012.09.008](https://doi.org/10.1016/j.astropartphys.2012.09.008) (cited on pages 5, 23).
- [13] D. Chirkin and W. Rhode. "Propagating leptons through matter with Muon Monte Carlo (MMC)". In: (July 2004) (cited on page 5).
- [14] L. Raedel. "Simulation Studies of the Cherenkov Light Yield from Relativistic Particles in High-Energy Neutrino Telescopes with Geant4". MA thesis. Aachen, Germany: Rheinisch-Westfälischen Technischen Hochschule, 2012 (cited on pages 5, 6).
- [15] M. Tanabashi et al. "Review of Particle Physics". In: *Phys. Rev. D* 98 (3 Aug. 2018), p. 030001. doi: [10.1103/PhysRevD.98.030001](https://doi.org/10.1103/PhysRevD.98.030001) (cited on page 6).
- [16] S. Agostinelli et al. "Geant4—a simulation toolkit". In: *Nucl. Instr. Meth. Phys. Res.* 506.3 (July 2003), pp. 250–303. doi: [10.1016/s0168-9002\(03\)01368-8](https://doi.org/10.1016/s0168-9002(03)01368-8) (cited on pages 6, 23).

- [17] T. Gabriel et al. "Energy dependence of hadronic activity". In: *Nuclear Instruments and Methods in Physics Research Section A: Accelerators, Spectrometers, Detectors and Associated Equipment* 338.2 (1994), pp. 336–347. doi: [https://doi.org/10.1016/0168-9002\(94\)91317-X](https://doi.org/10.1016/0168-9002(94)91317-X) (cited on page 6).
- [18] A. Terliuk. "Measurement of atmospheric neutrino oscillations and search for sterile neutrino mixing with IceCube DeepCore". PhD thesis. Berlin, Germany: Humboldt-Universität zu Berlin, Mathematisch-Naturwissenschaftliche Fakultät, 2018. doi: 10.18452/19304 (cited on page 7).
- [19] L. Fischer. https://github.com/LeanderFischer/icetray_double_cascade_generator_functions (cited on page 9).
- [20] R. Abbasi et al. "LeptonInjector and LeptonWeighter: A neutrino event generator and weighter for neutrino observatories". In: *Comput. Phys. Commun.* 266 (2021), p. 108018. doi: 10.1016/j.cpc.2021.108018 (cited on page 12).
- [21] P. Coloma et al. "GeV-scale neutrinos: interactions with mesons and DUNE sensitivity". In: *Eur. Phys. J. C* 81.1 (2021), p. 78. doi: 10.1140/epjc/s10052-021-08861-y (cited on pages 13, 15, 16).
- [22] J. Alwall et al. "The automated computation of tree-level and next-to-leading order differential cross sections, and their matching to parton shower simulations". In: *JHEP* 07 (2014), p. 079. doi: 10.1007/JHEP07(2014)079 (cited on page 13).
- [23] C. Argüelles. <https://github.com/arguelles/NuXSSplMkr> (cited on page 13).
- [24] J.-M. Levy. "Cross-section and polarization of neutrino-produced tau's made simple". In: *J. Phys. G* 36 (2009), p. 055002. doi: 10.1088/0954-3899/36/5/055002 (cited on page 14).
- [25] E. Tiesinga et al. "CODATA recommended values of the fundamental physical constants: 2018". In: *Rev. Mod. Phys.* 93 (2 July 2021), p. 025010. doi: 10.1103/RevModPhys.93.025010 (cited on page 15).
- [26] <https://github.com/icecube/pisa> (cited on page 17).
- [27] R. Abbasi et al. "Measurement of atmospheric neutrino mixing with improved IceCube DeepCore calibration and data processing". In: *Phys. Rev. D* 108 (1 July 2023), p. 012014. doi: 10.1103/PhysRevD.108.012014 (cited on pages 21, 28, 29, 32, 34).
- [28] M. Honda et al. "Atmospheric neutrino flux calculation using the NRLMSISE-00 atmospheric model". In: *Phys. Rev. D* 92 (2 July 2015), p. 023004. doi: 10.1103/PhysRevD.92.023004 (cited on page 22).
- [29] C. Andreopoulos et al. "The GENIE Neutrino Monte Carlo Generator: Physics and User Manual". In: (2015) (cited on pages 23, 33).
- [30] M. Glück, E. Reya, and A. Vogt. "Dynamical parton distributions revisited". In: *The European Physical Journal C* 5 (Sept. 1998), pp. 461–470. doi: 10.1007/s100529800978 (cited on page 23).
- [31] A. Bodek and U. K. Yang. "Higher twist, xi(omega) scaling, and effective LO PDFs for lepton scattering in the few GeV region". In: *Journal of Physics G: Nuclear and Particle Physics* 29.8 (2003), p. 1899. doi: 10.1088/0954-3899/29/8/369 (cited on page 23).
- [32] J.-H. Koehne et al. "PROPOSAL: A tool for propagation of charged leptons". In: *Computer Physics Communications* 184.9 (2013), pp. 2070–2090. doi: <https://doi.org/10.1016/j.cpc.2013.04.001> (cited on page 23).
- [33] Y. Becherini et al. "A parameterisation of single and multiple muons in the deep water or ice". In: *Astroparticle Physics* 25.1 (2006), pp. 1–13. doi: <https://doi.org/10.1016/j.astropartphys.2005.10.005> (cited on page 23).
- [34] D. Heck et al. "CORSIKA: A Monte Carlo code to simulate extensive air showers". In: (Feb. 1998) (cited on page 23).
- [35] T. K. Gaisser. "Spectrum of cosmic-ray nucleons, kaon production, and the atmospheric muon charge ratio". In: *Astropart. Phys.* 35 (2012), pp. 801–806. doi: 10.1016/j.astropartphys.2012.02.010 (cited on page 23).
- [36] R. Engel et al. "The hadronic interaction model Sibyll – past, present and future". In: *EPJ Web Conf.* 145 (2017). Ed. by B. Pattison, p. 08001. doi: 10.1051/epjconf/201614508001 (cited on page 23).
- [37] C. Kopper et al. <https://github.com/claudiok/clsim> (cited on page 24).

- [38] D. Chirkin et al. "Photon Propagation using GPUs by the IceCube Neutrino Observatory". In: *2019 15th International Conference on eScience (eScience)*. 2019, pp. 388–393. doi: 10.1109/eScience.2019.00050 (cited on page 24).
- [39] M. G. Aartsen et al. "Measurement of South Pole ice transparency with the IceCube LED calibration system". In: *Nucl. Instrum. Meth. A* 711 (2013), pp. 73–89. doi: 10.1016/j.nima.2013.01.054 (cited on page 24).
- [40] A. Trettin. "Search for eV-scale sterile neutrinos with IceCube DeepCore". PhD thesis. Berlin, Germany: Humboldt-Universität zu Berlin, Mathematisch-Naturwissenschaftliche Fakultät, 2023. doi: <https://github.com/atrettin/PhD-Thesis> (cited on pages 24, 25, 35).
- [41] G. Mie. "Beiträge zur Optik trüber Medien, speziell kolloidaler Metallösungen". In: *Annalen der Physik* 330.3 (1908), pp. 377–445. doi: <https://doi.org/10.1002/andp.19083300302> (cited on page 24).
- [42] L. G. Henyey and J. L. Greenstein. "Diffuse radiation in the Galaxy." In: *apj* 93 (Jan. 1941), pp. 70–83. doi: 10.1086/144246 (cited on page 24).
- [43] S. Fiedlschuster. "The Effect of Hole Ice on the Propagation and Detection of Light in IceCube". In: (Apr. 2019) (cited on page 24).
- [44] M. G. Aartsen et al. "In-situ calibration of the single-photoelectron charge response of the IceCube photomultiplier tubes". In: *Journal of Instrumentation* 15.6 (June 2020), P06032. doi: 10.1088/1748-0221/15/06/P06032 (cited on page 25).
- [45] M. Larson. "Simulation and Identification of Non-Poissonian Noise Triggers in the IceCube Neutrino Detector". Available at <https://ir.ua.edu/handle/123456789/1927>. MA thesis. University of Alabama, Tuscaloosa, AL, USA, 2013 (cited on page 25).
- [46] M. Larson. "A Search for Tau Neutrino Appearance with IceCube-DeepCore". available at https://discoverycenter.nbi.ku.dk/teaching/thesis_page/mjlarson_thesis.pdf. PhD thesis. University of Copenhagen, Denmark, 2018 (cited on page 25).
- [47] E. Lohfink. "Testing nonstandard neutrino interaction parameters with IceCube-DeepCore". PhD thesis. Mainz, Germany: Johannes Gutenberg-Universität Mainz, Fachbereich für Physik, Mathematik und Informatik, 2023. doi: <http://doi.org/10.25358/openscience-9288> (cited on page 25).
- [48] M. G. Aartsen et al. "The IceCube Neutrino Observatory: Instrumentation and Online Systems". In: *JINST* 12.03 (2017), P03012. doi: 10.1088/1748-0221/12/03/P03012 (cited on page 26).
- [49] J. H. Friedman. "Stochastic gradient boosting". In: *Computational Statistics & Data Analysis* 38 (2002), pp. 367–378 (cited on page 27).
- [50] R. Abbasi et al. "Low energy event reconstruction in IceCube DeepCore". In: *Eur. Phys. J. C* 82.9 (2022), p. 807. doi: 10.1140/epjc/s10052-022-10721-2 (cited on page 29).
- [51] S. Yu and J. Micallef. "Recent neutrino oscillation result with the IceCube experiment". In: *38th International Cosmic Ray Conference*. July 2023 (cited on page 29).
- [52] S. Yu and on behalf of the IceCube collaboration. "Direction reconstruction using a CNN for GeV-scale neutrinos in IceCube". In: *Journal of Instrumentation* 16.11 (2021), p. C11001. doi: 10.1088/1748-0221/16/11/C11001 (cited on pages 29, 30).
- [53] J. Micallef. <https://github.com/jessimic/LowEnergyNeuralNetwork> (cited on page 29).
- [54] M. Huennefeld. "Deep Learning in Physics exemplified by the Reconstruction of Muon-Neutrino Events in IceCube". In: *PoS ICRC2017* (2017), p. 1057. doi: 10.22323/1.301.1057 (cited on page 29).
- [55] H. Dembinski et al. "Data-driven model of the cosmic-ray flux and mass composition from 10 GeV to 10^{11} GeV". In: *PoS ICRC2017* (2017), p. 533. doi: 10.22323/1.301.0533 (cited on page 32).
- [56] G. D. Barr et al. "Uncertainties in atmospheric neutrino fluxes". In: *Phys. Rev. D* 74 (9 Nov. 2006), p. 094009. doi: 10.1103/PhysRevD.74.094009 (cited on page 32).
- [57] J. Evans et al. "Uncertainties in atmospheric muon-neutrino fluxes arising from cosmic-ray primaries". In: *Phys. Rev. D* 95 (2 Jan. 2017), p. 023012. doi: 10.1103/PhysRevD.95.023012 (cited on page 32).
- [58] A. Fedynitch et al. <https://github.com/afedynitch/MCEq> (cited on page 32).

- [59] G. D. Barr et al. "Uncertainties in Atmospheric Neutrino Fluxes". In: *Phys. Rev. D* 74 (2006), p. 094009. doi: 10.1103/PhysRevD.74.094009 (cited on page 32).
- [60] F. Riehn et al. "Hadronic interaction model sibyll 2.3d and extensive air showers". In: *Phys. Rev. D* 102 (6 Sept. 2020), p. 063002. doi: 10.1103/PhysRevD.102.063002 (cited on page 32).
- [61] A. Cooper-Sarkar, P. Mertsch, and S. Sarkar. "The high energy neutrino cross-section in the Standard Model and its uncertainty". In: *JHEP* 08 (2011), p. 042. doi: 10.1007/JHEP08(2011)042 (cited on page 33).
- [62] Q. Wu et al. "A precise measurement of the muon neutrino–nucleon inclusive charged current cross section off an isoscalar target in the energy range $2.5 < E < 40$ GeV by NOMAD". In: *Physics Letters B* 660.1 (2008), pp. 19–25. doi: <https://doi.org/10.1016/j.physletb.2007.12.027> (cited on page 34).
- [63] M. M. Tzanov. "Precise measurement of neutrino and anti-neutrino differential cross sections on iron". PhD thesis. University of Pittsburgh, Pennsylvania, Jan. 2005 (cited on page 34).
- [64] W. G. Seligman. "A next-to-leading-order QCD analysis of neutrino-iron structure functions at the Tevatron". PhD thesis. Columbia University, New York, Aug. 1997 (cited on page 34).
- [65] Rongen, Martin. "Measuring the optical properties of IceCube drill holes". In: *EPJ Web of Conferences* 116 (2016), p. 06011. doi: 10.1051/epjconf/201611606011 (cited on page 34).